**Article type:** Standard Paper

# Increasing drought effects on five European pines modulate $\Delta^{13}C$-growth coupling along a Mediterranean altitudinal gradient

T.A. Shestakova[a*], J.J. Camarero[b], J.P. Ferrio[c,d], A.A. Knorre[e], E. Gutiérrez[a], and J. Voltas[c]

[a]Department of Evolutionary Biology, Ecology and Environmental Sciences, University of Barcelona, E-08028 Barcelona, Spain

[b]Pyrenean Institute of Ecology, IPE-CSIC, E-50059 Zaragoza, Spain

[c]Department of Crop and Forest Sciences – AGROTECNIO Center, University of Lleida, E-25198 Lleida, Spain

[d]Department of Botany, University of Concepcion, 4030000 Concepción, Chile

[e]Department of Forestry, Siberian Federal University, 660041 Krasnoyarsk, Russia

[*]Corresponding Author:

Tatiana A. Shestakova

Department of Evolutionary Biology, Ecology and Environmental Sciences

University of Barcelona

Av. Diagonal 643, E-08028 Barcelona, Spain

e-mail: tasha.work24@gmail.com

**Running headline:** Rising $\Delta^{13}$C-growth coupling in Mediterranean pines

**Word count** (summary, main text and references): 7,498 words

## Summary

1. Climate warming increases vulnerability to drought in Mediterranean water-limited forests. However, we still lack knowledge of the long-term physiological responses of coexisting pine species in these forests regarding their ability to cope with warming-induced drought stress.

2. We investigated spatiotemporal patterns of tree performance for five isohydric pines with partially overlapping ecological niches in the eastern Iberian Peninsula along an altitudinal gradient: *Pinus halepensis* = *P. pinaster* ≤ *P. nigra* ≤ *P. sylvestris* ≤ *P. uncinata*.

3. Using indexed tree-ring widths ($TRW_i$) we assessed changes in temporal coherence of radial growth (growth synchrony, $\hat{a}_C$) over the period 1902–2011 across three elevation belts: low ≈ 1100 m; mid = 1615 m; high = 2020 m. We also examined by mixed modelling whether $TRW_i$ showed an increased coupling with leaf-level gas exchange (inferred from indexed carbon isotope discrimination, $\Delta^{13}C_i$) by enhanced stomatal regulation in response to an amplified regional drought stress.

4. Increasingly negative annual water balances (decrease in annual precipitation minus evapotranspiration = –4.8 mm $year^{-1}$; 1970–2011) prompted more synchronous growth of coexisting pines between low- and mid-elevation belts, with $\hat{a}_C$ rising from 0.25 ± 0.04 (1902–1951) to 0.62 ± 0.05 (1962–2011). This effect was coupled with tighter stomatal regulation at mid-elevation as indicated by high correlations between $TRW_i$ and $\Delta^{13}C_i$ (>0.60 from the mid-1970s onwards) which resembled those found at low-elevation. Simultaneously, $TRW_i$ *vs*. $\Delta^{13}C_i$ uncoupling occurred at the high-elevation belt across species.

5. Weaker growth-climate relationships as elevation increased highlighted the major role of the altitude-dependent thermal gradient in growth responsiveness to drought; however, an intensified $\Delta^{13}C_i$ response to spring water availability across elevation belts observed from mid-1970s onwards suggested regional shifts in tree physiological activity linked to earlier seasonal drought impacts. Warming-induced drought stress is spreading to higher altitudes in Iberian pinewoods as multispecies growth is linked to progressively tighter stomatal control of water losses reflected in wood $\Delta^{13}C$.

**Keywords:** carbon isotopes, climate warming, dendroecology, mixed modelling, *Pinus*, tree rings

## Introduction

Understanding climate influences on forest ecosystems is crucial in a global warming context, especially in exposed areas such as the Mediterranean Basin (IPCC 2013). In lowland Mediterranean ecosystems, forest growth is primarily constrained by water availability. In Mediterranean mountain forests, however, trees are subjected to varying degrees of water stress depending on their position along altitudinal gradients and the modulation exerted by topography-controlled variation in temperature and soil moisture (Bunn, Waggoner & Graumlich 2005). This leads to distinct growth-climate associations depending on whether drought or low temperature is the predominant factor controlling tree performance (Sánchez-Salguero *et al*. 2015).

In dendrochronology the conventional premise stating that site-level growth-climate relationships are stable over time (Hughes *et al*. 1982) is challenged based on how trees are reacting to warming (DeSoto *et al*. 2012). For instance, increasingly negative impacts of summer heat and drought on radial growth along with more favourable effects of warm winter conditions have been reported for mesic Iberian pinewoods during the past decades (Andreu *et al*. 2007). Thus, unravelling growth responses to climate along altitudinal gradients may provide clues on how forests are reacting to emerging combinations of temperature and precipitation under climate warming.

Despite the available wealth of dendroecological archives, we still lack knowledge on the long-term responses of coexisting species, which would be valuable to contextualise the impacts of ongoing climate change (Lévesque *et al*. 2013). However, there are indications of regionally coherent multispecies responses to climate change imprinted in tree rings (Shestakova *et al*. 2016). This especially holds where

growth is mainly constrained by few climate factors, as it is the case for circum-Mediterranean forests that are being subjected to increasing water shortage (Galván *et al*. 2015).

Most dendroecological studies rely on radial growth to assess climate change effects on long-term tree performance; however, additional information on leaf-level physiology can be gained through analysis of stable isotopes in tree rings (McCarroll & Loader 2004). Particularly, the ratio of the heavy to light carbon isotopes ($^{13}C/^{12}C$) depends on factors affecting $CO_2$ uptake, mainly controlled by photosynthetic rate ($A$) and stomatal conductance ($g_s$), as expressed in the ratio $A/g_s$ (intrinsic water-use efficiency, $WUE_i$; Farquhar, Ehleringer & Hubick 1989). In water-limited environments, carbon isotope discrimination ($\Delta^{13}C$) in tree rings can be mostly explained by the stomatal regulation of $CO_2$ fluxes into the leaf, integrating any environmental variable affecting stomatal conductance (Gessler *et al*. 2014). This is particularly true for isohydric species, like pines, which rapidly close stomata to avoid water losses, hence reducing carbon uptake but maintaining relatively constant leaf water potentials regardless of drought intensity (Klein 2014). Under such conditions, radial growth and $\Delta^{13}C$ are bound together by two factors: stomatal control and water availability. However, $\Delta^{13}C$ is also affected by changes in photosynthetic activity associated to irradiance, nutritional stresses, atmospheric N deposition or phenology when water becomes less limiting (Livingston *et al*. 1998). By combining ring-width and $\Delta^{13}C$, information can be gained on tree performance underlying biogeographical interactions, as these traits share spatial responses to drought events (Voelker *et al*. 2014).

Here, we analyse the response patterns to climate of five widely distributed European pines with partially overlapping distribution ranges along an altitudinal gradient of *ca.* 1000 m in the Gúdar range (eastern Spain). This small area (*ca*. 250 $km^2$) offers a unique opportunity to test the effects of global change on Mediterranean forests, as most Iberian pines coexist at different elevations. They belong to two clades of Eurasian pines (Price, Liston & Strauss 1998): the Mediterranean clade (= *pinaster*) (*P. halepensis* and *P. pinaster*) and the Eurosiberian clade (= *sylvestres*) (*P. nigra*, *P. sylvestris* and *P. uncinata*), which have different life histories and ecological requirements (Tapias *et al*. 2004). *P. halepensis* and *P. pinaster* are present at low elevations (up to 1200 m a.s.l.) and are subjected to prolonged summer drought. In contrast, *P. sylvestris* and *P. uncinata* are found above 1500 m and 1800 m a.s.l., respectively, in cold environments with a relatively short, dry summer. In turn, *P. nigra* is distributed in sub-Mediterranean transitional areas (1100–1600 m a.s.l.), forming mixed stands with *P. pinaster* and *P. sylvestris* at low and mid elevations, respectively. Within the Iberian Peninsula, *P. pinaster* has the broadest ecological niche (from sea level to 1900 m), followed by *P. nigra* (though being less tolerant of high temperature and drought; Matías *et al*. 2016). The other species, despite large distribution ranges, are confined to comparatively narrow environments. In Gúdar, *P. uncinata* is at the trailing edge of its natural range.

We hypothesise that increasing drought stress in the Gúdar range homogenized climate responses among pine species over the last 60 years, as drought effects spread from low to high elevations. At low-elevation sites, we expect a consistent positive relationship between growth and $\Delta^{13}C$ throughout the tree-ring record. Under such conditions, lower $\Delta^{13}C$ (higher $WUE_i$) during dry years would be mainly due to

stomatal-limited photosynthesis, hence associated to reduced assimilation, reflecting a conservative water use as a result of long-term adaptation and acclimation to drought. Conversely, we predict a weaker relationship between growth and $\Delta^{13}C$ upwards along the gradient but a gradual convergence at mid- and low-elevation sites, as the stomatal sensitivity to drought becomes more limiting for carbon uptake in isohydric pines. Consequently, we anticipate more synchronous growth driven by convergent stomatal responses across species as the climate becomes warmer and drier along the altitudinal gradient.

## Materials and methods

*Study area and field sampling*

The study was performed in natural pine forest stands located in Gúdar, Iberian System, eastern Spain (see Fig. S1 in Supporting Information). The area has a continental Mediterranean climate with two precipitation maxima in spring and autumn. Mean annual precipitation (MAP) is 636 mm (summer precipitation ≈ 100 mm) and mean annual temperature (MAT) is +8.3°C, with January being the coldest (+0.9°C) and July the warmest month (+17.9°C) (period 1950–2011, European high-resolution climate dataset, E-OBS; Haylock *et al.* 2008). However, climate conditions vary with altitude, ranging from relatively warm, drought-prone environments at low elevations to cold and humid sites at higher elevations (Fig. S2). Soils in the area are classified as Calcic Cambisols (FAO 1981). They have a calcium horizon within approx. 75–90 cm of the surface, are clayey or loamy textured and have low water holding capacity.

Field work was conducted in summer 2012 along an altitudinal gradient ranging from 1090 m up to 2020 m a.s.l. (the highest peak in the Gúdar range). Five pines

158 dominating different elevation belts were subjected to stratified sampling according to
159 the distribution range of each species: *P. halepensis* Mill., *P. nigra* Arn. subsp.
160 *salzmannii* (Dunal) Franco, *P. pinaster* Ait., *P. sylvestris* L. and *P. uncinata* Ram. (Fig.
161 S1, Table 1). Altogether, four open pine stands made up of individuals of similar size
162 and corresponding to three altitudinal belts (low ≈ 1100 m a.s.l., mid = 1615 m a.s.l. and
163 high = 2020 m a.s.l.) were sampled with the following species representation: *P.*
164 *halepensis* (low-elevation site, LS1), *P. pinaster* and *P. nigra* (LS2), *P. nigra* and *P.*
165 *sylvestris* (mid-elevation site, MS) and *P. sylvestris* and *P. uncinata* (high-elevation site,
166 HS) (Table 1). These sites did not show visible human or natural disturbances (e.g.,
167 stumps, fire scars). The range of climate variation between low- and high-elevation sites
168 was estimated to be 5.6°C (4.9–10.5°C) for MAT and 439 mm (465–904 mm) for MAP
169 (Appendix S1; Fig. S2).

170 Twenty mature, dominant and healthy trees were randomly selected per site and
171 species and their size was measured (diameter at breast height and total height using a
172 clinometer). Two cores were extracted at 1.30 m from cross-slope sides of the trunk
173 whenever possible using a 5-mm diameter borer. These samples were complemented
174 with data compiled from a previous study (Camarero *et al*. 2015a) in which the same
175 forest stands and slope aspects (but different trees) were sampled in summer 2006
176 following the same protocol. A total of 508 increment cores from 254 living pines were
177 collected along the gradient (Table 2). Both cores collected in 2006, together with one
178 core collected in 2012, were used for ring dating, while the second core sampled in
179 2012 was kept intact for isotope analysis.

180

181 *Sample preparation and ring-width measurements*

For tree-ring dating, samples were oven-dried at 60°C for 48 h and sanded until tree rings were clearly visible under a binocular microscope. Tree rings were visually cross-dated and measured with precision of 0.01 mm using a Lintab system (Fig. S3a). Cross-dating was verified with the COFECHA program (Holmes 1983). Tree-ring series were then used to build indexed tree-ring width ($TRW_i$) chronologies for each site and species (Appendix S1; Fig. S3b). The quality of the resulting chronologies was evaluated by calculation of the mean interseries correlation (*Rbar*) and the Expressed Population Signal (*EPS*) statistics. The study period was 1902–2011 (period with *EPS* > 0.85, except for *P. halepensis*) (Table 2). Trees sampled in 2012 were considered to provide a reliable representation of the period 2006–2011 (they amounted to 55% of the total number of trees). Besides, the annual basal area increment (BAI) was used to characterize absolute radial growth trends for the set of cross-dated trees for each site and species (Appendix S1).

*Carbon isotope analysis*

The five best cross-dated trees per site and species sampled in 2012 were selected for isotope measurements. Tree rings were split with annual resolution for the period 1950–2011, which was considered a reliable common time span for all tree-ring chronologies (i.e., excluding at least the first 30 years to avoid juvenile effects; Table 2). Rings corresponding to the same year, site and species were pooled into a single sample before analysis (Leavitt 2008), except every ten years (1951, 1961, …, 2011) for which rings were analysed individually to estimate between-tree variability in carbon isotopes (Appendix S1). The resulting samples were homogenised with a ball mill (Retsch MM301, Haan, Germany). Then, 0.30–0.40 mg of dry wood was weighed into tin foil

capsules and combusted to $CO_2$ using a Flash EA-1112 analyser interfaced with a Finnigan MAT Delta isotope ratio mass spectrometer (Thermo Fisher Scientific Inc., MA, USA). Isotope ratios were expressed as per mil deviations using the δ notation relative to Vienna Pee Dee Belemnite (VPDB). The accuracy of the analyses (SD of standards) was 0.06‰.

To account for changes in $\delta^{13}C$ of atmospheric $CO_2$ ($\delta^{13}C_{air}$), we calculated carbon isotope discrimination ($\Delta^{13}C$) from $\delta^{13}C_{air}$ and wood $\delta^{13}C$ ($\delta^{13}C$) (Fig. S4a) following Farquhar *et al*. (1989):

$$\Delta^{13}C = \frac{\delta^{13}C_{air} - \delta^{13}C}{1 + \delta^{13}C} \quad \text{(eqn 1)}$$

$\delta^{13}C_{air}$ applied to the samples varied between −8.28‰ and −6.94‰ (period 1950–2011) (Ferrio *et al.* 2005). Using $\Delta^{13}C$ records, intrinsic water-use efficiency ($WUE_i$) was estimated following standard procedures (Appendix S1).

Indexed $\Delta^{13}C$ chronologies ($\Delta^{13}C_i$) were obtained following the same procedure used for $TRW_i$ (Appendix S1; Fig. S4b). *Rbar* and *EPS* statistics were used to estimate the internal coherence of each chronology using the subset of years ($n$ = 7) in which individual $\Delta^{13}C$ records were available (Table 2). Both $TRW_i$ and $\Delta^{13}C_i$ chronologies were used as input for statistical analyses.

*Meteorological data*

As long-term regional instrumental records are scarce, estimates of climate variables (temperature, precipitation) were obtained from the nearest 0.25º-grid point (40°23'N, 0°38'W) of E-OBS (Haylock *et al.* 2008). A proxy of water availability was calculated as the difference between precipitation and potential evapotranspiration (P-PET), which approximates the water budget on an annual or monthly basis. PET was

estimated following Hargreaves & Samani (1982). Monthly mean temperature, precipitation and the Standardised Precipitation-Evapotranspiration Index (SPEI, a multiscalar drought index; Vicente-Serrano, Beguería & López-Moreno 2010) were used to assess relationships between $TRW_i$ or $\Delta^{13}C_i$ and climate. SPEI was calculated at time scales of one- (abbreviated as SPEI1), three- (SPEI3) and six-months (SPEI6) to monitor droughts with respect to different usable water resources.

*Statistical analysis*

**Long-term trends in $TRW_i$ patterns.** The quantification of common $TRW_i$ variability among chronologies (common signal strength or synchrony, $\hat{a}_C$) and of temporal changes in this common variability (changes in synchrony) were investigated over the period 1902–2011 through: (*i*) principal component analysis and (*ii*) variance-covariance (VCOV) modelling following Shestakova *et al.* (2014) (Appendix S1).

**Relationships between $TRW_i$ and $\Delta^{13}C_i$.** A bivariate random model was used to simultaneously take into account the information available on $TRW_i$ and $\Delta^{13}C_i$. This allowed for an estimation of the temporal association between these traits. Briefly, the correlation of year effects ($r_Y$) between traits 1 and 2 can be expressed as:

$$r_Y = \frac{\sigma_{Y_{12}}}{\sqrt{\sigma^2_{Y_1} \times \sigma^2_{Y_2}}} \quad \text{(eqn 2)}$$

where $\sigma_{Y_{12}}$ is the variability of year effects shared by traits 1 and 2 (covariance) across chronologies, and $\sigma^2_{Y_1}$ and $\sigma^2_{Y_2}$ stand for the variance component of year effects for traits 1 and 2 respectively. Following eqn (eqn 2), we calculated the correlation of year effects between $TRW_i$ and $\Delta^{13}C_i$ chronologies (and their standard errors) for each altitudinal

252 belt. These relationships were calculated for 25-year periods lagged by one year starting
253 in 1950. For details see Appendix S1.

254 **Development of master chronologies.** A master chronology corresponding to
255 each altitudinal belt was obtained for either $TRW_i$ or $\Delta^{13}C_i$ by *best linear unbiased*
256 *prediction* (BLUP) of year effects (Shestakova *et al*. 2016). BLUP increases accuracy
257 relative to ordinary least squares methods (i.e. standard Analysis of Variance) and
258 maximises the correlation between true and predicted values associated to the random
259 (year) effect. BLUPs were estimated for the period 1950–2011 using eqn (eqn 4) in
260 Appendix S1 and were subsequently used as inputs for climate analysis.

261 **Relationships between tree-ring traits and climate.** Pearson correlations were
262 calculated for the period 1950–2011 to quantify climate-trait relationships on a monthly
263 basis for each altitudinal belt. Temporal stability of these associations was assessed
264 through moving correlations for 25-year segments lagged by one year. The presence of
265 overlapping climatic information present in $TRW_i$ and $\Delta^{13}C_i$ was controlled through
266 partial correlation analysis. Climate relationships were analysed from the previous
267 October to September of the year of tree-ring formation.

268

269 ## Results

270 *Regional climate trends*

271 There was a consistent warming since 1970 (+1.8°C absolute increase; Fig. 1a),
272 which was particularly evident for the growing season (+2.8°C in spring; +2.6°C in
273 summer) (Fig. 1b). Precipitation showed high interannual variability (Fig. 1a), with the
274 last four decades being slightly drier than the preceding period (1950–1970) (average
275 7% decrease in precipitation). Annual P-PET estimates were mostly negative over the

276 period 1950–2011 and exhibited a significant decrease since 1970 (slope = –4.8 mm
277 year$^{-1}$), indicating an intensifying impact of warming-induced drought stress (Fig. 1a).
278 This effect was particularly noticeable in March, June and July (Fig. 1b).
279
280 *Tree-ring width patterns*
281 The loadings of the first (PC1) and second (PC2) principal components
282 accounted for 59.7% and 23.6% of the total variance in $TRW_i$ variability, respectively
283 (Fig. 2a). All chronologies had positive PC1 loadings, suggesting a common climate
284 signal along the gradient. However, high-elevation *P. sylvestris* and *P. uncinata*
285 chronologies had positive PC2 loadings, while low-elevation *P. halepensis*, *P. nigra* and
286 *P. pinaster* chronologies had negative PC2 loadings. In turn, mid-elevation *P. nigra* and
287 *P. sylvestris* chronologies had nearly zero PC2 loadings. Such ordination of
288 chronologies along PC2 suggested the existence of three temporal $TRW_i$ patterns
289 concomitant to each altitudinal belt. These patterns were supported by weaker (albeit
290 significant) correlations found between chronologies belonging to different belts as
291 compared to those of the same belt (Table S1).
292 The degree of synchronous growth was then examined among and within
293 altitudinal belts. Synchrony was high at the between-belt ($\hat{a}_{Cb}$) and, especially, at the
294 within-belt level ($\hat{a}_{Cw}$). The highest synchrony involved *P. sylvestris* and *P. uncinata* at
295 HS ($\hat{a}_{Cw}$ = 0.90 ± 0.01; mean ± SE), followed by *P. nigra* and *P. sylvestris* at MS (0.80
296 ± 0.02) and *P. halepensis*, *P. nigra* and *P. pinaster* at LS (0.68 ± 0.03). At the between-
297 belt level, $\hat{a}_{Cb}$ decreased with increasing altitudinal difference: synchrony was similar
298 between neighbouring belts ($\hat{a}_{Cb}$ = 0.50 ± 0.03 and 0.41 ± 0.03 for LS/MS and MS/HS,
299 respectively), whereas it was weaker between altitudinal extremes (0.22 ± 0.02 for

LS/HS). The regional synchrony for the complete set of chronologies ($\hat{a}_C$ = 0.46 ± 0.03) was slightly lower than that observed among trees within a site ($\bar{R}bar$ = 0.56 ± 0.04).

*Temporal trends in regional growth synchrony*

The regional synchrony showed a steady increase over the period 1902–2011 (slope = 0.013 year$^{-1}$; $P$ < 0.001) (Fig. 2b, upper panel), rising from 0.33 ± 0.04 in 1902–1951 to 0.49 ± 0.05 in 1962–2011 (value non-significantly different from $\bar{R}bar$). However, the temporal evolution of synchrony between pairs of elevation belts ($\hat{a}_{Cb}$) was inconsistent (Fig. 2b, lower panel). LS and MS showed a significant increase in synchrony (slope = 0.025 year$^{-1}$; $P$ < 0.001), rising from 0.25 ± 0.04 (1902–1951) to 0.62 ± 0.05 (1962–2011). Conversely, synchrony changes between LS and HS and between MS and HS showed no clear temporal trend. These patterns were unaffected by the rigidity of the splines used for chronology building (Fig. S5).

*Temporal trends in $TRW_i$ vs. $\Delta^{13}C_i$ relationships*

The correlation between pairs of $\Delta^{13}C_i$ chronologies was always significant, but higher between chronologies belonging to neighbouring belts (Table S1). Similarly, we found strong, although geographically-structured, correlations of year effects ($r_Y$) between $TRW_i$ and $\Delta^{13}C_i$ over the period 1950–2011, which decreased with altitude. The highest value was observed at LS ($r_Y$ = 0.83 ± 0.06), followed by MS ($r_Y$ = 0.59 ± 0.12) and HS ($r_Y$ = 0.42 ± 0.12). These relationships, however, started to diverge at MS and HS during the 1970s (Fig. 3). On the one hand, the association strengthened at MS, reaching statistically equivalent values to those found at the lowest altitudinal belt; conversely, it became non-significant at HS. These changing patterns differed from the

consistently strong association found between $TRW_i$ and $\Delta^{13}C_i$ at LS (Fig. S6), which fluctuated within a narrow range over the study period ($r_Y > 0.70$) (Fig. 3).

*Climate drivers of $TRW_i$ and $\Delta^{13}C_i$*

The relationships between either $TRW_i$ or $\Delta^{13}C_i$ and climate were structured along the altitudinal gradient, with trees responding in a similar way to variations in precipitation and SPEI1. Particularly, growth responses to climate were similar at LS and MS, although pines were more sensitive to climate fluctuations at LS (Fig. 4a). $TRW_i$ was enhanced by previous winter (December), spring and summer precipitation, and also by reduced drought stress (i.e., negative SPEI1) during the same months. Besides, growth was more sensitive to longer drought episodes (SPEI3 and SPEI6), especially occurring in May through August (i.e., when water deficit peaked). There were also significant relationships with February (positive) and summer temperature (negative). Moreover, $TRW_i$ correlated negatively with May temperature, but only at LS. Climate-growth associations were weaker at HS, where $TRW_i$ was associated with previous October (negatively) and current August precipitation and SPEI1 (positively) and also with April temperature (positively). Conversely, there were no significant associations between growth and either SPEI3 or SPEI6.

For $\Delta^{13}C_i$, there were positive and mostly significant monthly relationships with precipitation and SPEI1 along the gradient (except for the previous autumn) (Fig. 4b). Notably, the drought impacts were amplified at three- and six-month scales regardless of elevation belt. The highest correlations were found in spring at LS and MS and in summer at HS. In contrast, the temperature signal in $\Delta^{13}C_i$ was weaker, with negative associations from May–September (LS and MS) and from June–September (HS).

348

349 *Temporal trends of $TRW_i$ and $\Delta^{13}C_i$ associations with climate*

350 The associations between either $TRW_i$ or $\Delta^{13}C_i$ and climate were temporally
351 unstable (Fig. 5). At LS and MS, there was an increase in $TRW_i$ sensitivity to both
352 summer temperature (negative) and spring SPEI1 (positive). Particularly, we found a
353 significant negative correlation between $TRW_i$ and July temperature since the 1980s,
354 which later extended to June; likewise, there was a positive association with
355 temperature in February since the 1980s, which extended to January at the turn of the
356 century (LS) (Fig. 5a). Also, at LS and MS a positive correlation between $TRW_i$ and
357 May SPEI1 extended to June (since the 1980s) and April (since the 2000s) (Fig. 5b). At
358 HS, the initial positive correlation with May–June temperature shifted to April in recent
359 decades; also, a negative correlation with previous December temperature was detected
360 in the 1990s, which extended to January in the 2000s (Fig. 5a). We also found a
361 temporal shift in the association between $TRW_i$ and summer SPEI1, with significant
362 correlations in July–August from 1950 to 2000 but with no clear signal beyond that
363 (Fig. 5b).

364 $\Delta^{13}C_i$ sensitivity to late spring-early summer temperature was temporally
365 unstable at LS and MS, with significant negative correlations in May (1950–1980) and
366 June–July (1980–2000) (Fig. 5a). Positive correlations were also found with SPEI1 in
367 spring, September (until the 1990s) and the previous December (shifting to January in
368 the 2000s) (Fig. 5b). At HS, we found a shifted (negative) response of $\Delta^{13}C_i$ to
369 temperature over time, with significant correlations in August–September (1950–1990),
370 July (1970–1990) and June (from 2000 onwards) (Fig. 5a). There was also a positive

correlation with SPEI1 in July–September (shifting to June from 2000 onwards), February and April (until 1980) (Fig. 5b).

The tight association between $TRW_i$ and $\Delta^{13}C_i$ (decreasing upwards along the gradient) suggested the existence of overlapping climatic information in these traits. To check for such redundancy we evaluated the relationships between $TRW_i$ and climate after controlling for $\Delta^{13}C_i$ effects through partial correlation (Fig. S7). Thus, mainly winter and early summer temperature signals were preserved in $TRW_i$ records but only at HS: December–January (negative, from the 1990s) and April–June (positive, until the 1980s).

*Trends in BAI and $WUE_i$*

BAI showed decreasing trends since 1950 at HS and also for *P. nigra* at MS, while it significantly increased for *P. halepensis* (Fig. 6). In contrast, $WUE_i$ showed increasing trends for all site-species combinations (Fig. 6), ranging from 17% (*P. pinaster*) to 28% (*P. sylvestris* at HS) between the first (1950–1959) and the last decade examined (2002–2011). Changes in $WUE_i$ were negatively related to BAI, with the exception of *P. halepensis* and *P. nigra* at LS, which showed non-significant relationships (Fig. 6).

## Discussion

*Increasing regional coherence of $TRW_i$ patterns*

The steady increase in synchrony observed in Gúdar, peaking at the turn of the 21st century, supports our hypothesis of a progressively large-scale impact of drought effects on water-limited forests as the climate warms and dries. Gradually, low- and

mid-elevation trees grew more synchronously over the 20th century, suggesting that warming-induced growth limitations are spreading upwards in Mediterranean mountains (Galván *et al*. 2015). It is likely that drought is gaining relevance as factor controlling tree growth compared with the effect of local drivers (e.g., topography, nutrient availability) and is also increasing species' sensitivity to competition (Gómez-Aparicio *et al.* 2011). Indeed, the comparison between intra-site (i.e. local) correlation (mean *Rbar* across sites = 0.56) and present-day regional growth synchrony ($\hat{a}_C$ = 0.49) suggests local and climate effects of similar magnitude on multi-species growth variability in the area. Warming-induced enhanced synchrony has been reported in other Mediterranean forests: $\hat{a}_C$ = 0.44–0.58 before and after 1965, respectively, for *Pinus pinea* in central-south Iberian Peninsula (Natalini *et al*. 2015) and $\hat{a}_C$ = 0.19–0.24 before and after 1950, respectively, for three conifers in Spain (Shestakova *et al*. 2016). Also, the strong synchrony among species at each belt demonstrates highly coordinated growth responses to local conditions, especially at HS and MS for Eurosiberian pines ($\hat{a}_{Cw} \geq 0.80$), which is in agreement with their common morphophysiological features (e.g., Tapias *et al*. 2004). The comparatively lower synchrony recorded at LS ($\hat{a}_{Cw}$ = 0.68) is likely related to different stand characteristics (e.g., basal area; Table 2) for *P. halepensis* (LS1) and *P. pinaster* and *P. nigra* (LS2) which, together, comprised the low elevation belt.

*Temporal changes in $TRW_i$ vs. $\Delta^{13}C_i$ relationships depend on the altitudinal belt*

The increasingly positive association between $TRW_i$ and $\Delta^{13}C_i$ in mixed *P. nigra – P. sylvestris* stands at MS observed from the 1970s, reaching values comparable to those at LS, corroborates that drought is becoming the main climatic stressor within

419 the transitional area between low- and high-elevation forests, progressively constraining
420 assimilation through a tighter stomatal control of water losses. Both radial growth and
421 $\Delta^{13}C$ are influenced by water availability in drought-prone environments, so their
422 association increases in parallel with an enhanced frequency and intensity of drought
423 episodes. Hence, where $\Delta^{13}C$ is more responsive to variations in water availability,
424 $\Delta^{13}C_i$ and $TRW_i$ share a robust temporal signal, as shown at the regional level for *P.*
425 *halepensis* (del Castillo, Voltas & Ferrio 2015). In this regard, it is expected that pines
426 more exposed to drought (i.e., at low elevations) would show lower water potential
427 thresholds ($\Psi$) for stomatal closure than in more mesic sites (i.e., at higher elevations),
428 in order to maintain equivalent levels of gas exchange (Klein 2014). Species-specific
429 differences in stomatal sensitivity to water status agree with the distribution of pines
430 along the gradient, approaching stomatal closure at $\Psi_{leaf}$ = –3.5 to –2.8 MPa in *P.*
431 *halepensis* (Froux *et al*. 2005; Klein, Cohen & Yakir 2011), –2.0 to –1.6 MPa in *P.*
432 *nigra* (Froux *et al*. 2005), –1.5 to –1.2 MPa in *P. pinaster* (Picon, Guehl & Ferhi 1996)
433 and –1.4 to –1.0 MPa in *P. sylvestris* (Irvine *et al*. 1998). The higher species' sensitivity
434 to drought stress upwards along the gradient relates well to the recent increase in
435 coupling between $TRW_i$ and $\Delta^{13}C_i$ observed at mid-elevation for the more drought-
436 susceptible Eurosiberian species.

437 Conversely, the recent and sudden weakening of common $TRW_i$ and $\Delta^{13}C_i$
438 signals in high-elevation forests is intriguing and suggests an uncoupling of regulatory
439 mechanisms of water-carbon economy at the turn of this century. This phenomenon
440 might be explained by premature dehardening and associated embolism induced by the
441 combined effect of warmer temperatures, winter drought and cold spells, as observed in
442 nearby stands in the 2000s (Voltas *et al*. 2013). Further ecophysiological work (e.g.,

443 xylem anatomy, multi-isotopic approaches) would be needed to unveil the exact causes
444 of this phenomenon.
445
446 *The extent of distinct $TRW_i$ and $\Delta^{13}C_i$ responses to climate*
447 In mountain ecosystems, climate and forest productivity are strongly influenced
448 by elevation (Kienast *et al*. 1987). However, our results confirm that water shortage
449 occurring during the growing season (as indicated by SPEI) is a key factor limiting tree
450 performance along the Gúdar gradient. Yet it should be noted that the pine species did
451 not perfectly co-occur across altitudinal belts and the growth responses to drought were
452 not exactly coincident across belts. Weaker growth-climate relationships as elevation
453 increased highlight the major role of the altitude-dependent thermal gradient in growth
454 responsiveness to drought, although such altitudinal responses could partially overlap
455 with species-specific differences in physiological performance (Matías *et al.* 2016).
456 Topographic and soil characteristics may have further exacerbated such differences,
457 since the low- and mid-elevation forests were located on rocky slopes or on shallow
458 soils, whereas the high-elevation site was placed on a plateau with deeper soils. A
459 comprehensive soil sample design could be applied in order to confirm and quantify
460 such effects on tree performance.
461 Our findings indicate that drought starts earlier in the growing season at low and
462 mid elevations (i.e., driest sites). At high-elevation, tree growth is only sensitive to late
463 summer drought. These results agree with other studies indicating that pine growth is
464 mainly controlled by winter-spring precipitation in lowland Mediterranean forests (e.g.,
465 Pasho *et al*. 2011) and mostly influenced by summer water availability at high
466 elevations (>1500 m; Andreu *et al.* 2007). In Mediterranean forests, growth conditions

467 generally improve with elevation, reducing summer temperatures and water demand;
468 furthermore, snowmelt may also help to mitigate drought stress. In this regard,
469 enhanced growth after a wet winter–early spring highlights the importance of soil water
470 recharge prior to cambial activity in lowland forests (Pasho *et al*. 2011). The positive
471 growth responses to February (at low and mid elevations) and April temperature (at
472 high elevation) supports a key role of early-season temperatures in cambial resumption
473 after winter dormancy (Deslauriers *et al.* 2008).

474 We found stronger coherence of $\Delta^{13}C_i$ records along the gradient compared with
475 $TRW_i$, confirming that carbon isotopes are better tracers of regional drought signals
476 than radial growth (McCarroll & Loader 2004). Trees growing at high elevation were
477 the most $\Delta^{13}C_i$-responsive to summer precipitation, as previously reported in Spain
478 (Andreu *et al*. 2008) and in the French Alps (Gagen, McCarroll & Edouard 2006).
479 Conversely, $\Delta^{13}C_i$ was positively related to spring and early autumn precipitation at low
480 and mid elevations (del Castillo *et al*. 2015), suggesting that cambial activity slows
481 down during summer due to water shortage in sub-Mediterranean pinewoods (Voltas *et*
482 *al*. 2013). The high $\Delta^{13}C_i$-sensitivity to high summer temperatures across the gradient
483 points to decreased stomatal conductance as a result of high evaporative demand, hence
484 decreasing $\Delta^{13}C_i$ provided that the soil does not completely dry out (Saurer *et al*. 2008).
485 Furthermore, $\Delta^{13}C_i$ was positively associated with winter precipitation. Cold season
486 precipitation often falls as snow in Gúdar, determining the soil moisture status early in
487 the vegetative period. This condition may cause a lag between the period imprinted on
488 $\Delta^{13}C_i$ and the actual growing season (Holzkämper *et al*. 2008). Indeed, the climate
489 analysis reveals a delay in $TRW_i$ responses to precipitation compared to $\Delta^{13}C_i$,

490 suggesting that the latter may be more sensitive to changes in moisture (Hartl-Meier *et*
491 *al*. 2014).
492
493 *Interpreting temporal changes of $TRW_i$ and $\Delta^{13}C_i$ responses to warming*
494 Our results suggest that the conspicuous warming trend and reduced water
495 availability (i.e., more negative P-PET) are producing the following effects on sub-
496 Mediterranean (i.e. low- and mid-elevation) pinewoods: (*i*) appearance of a
497 temperature-sensitive growth period in late-winter, pointing to earlier cambial growth
498 onset perhaps favoured by advanced snowmelt; (*ii*) negative influence of peak summer
499 temperatures on growth and (*iii*) increasing dependence of tree performance on early
500 spring water availability (a wet season in the western Mediterranean). Specifically, an
501 intensified $\Delta^{13}C_i$ response to SPEI in early spring could be a consequence of more
502 recurrent and prolonged drought episodes suggested by negative P-PET trends in
503 March, June and July. These effects support our hypothesis that increasing drought
504 stress is responsible for the strong growth synchrony currently observed for the area.
505 At high elevations, low summer temperatures did not constrain growth, hence
506 challenging the assumption that productivity is temperature-limited in Mediterranean
507 high-mountain ecosystems (Galván *et al*. 2015). Instead, a recent shift in $\Delta^{13}C_i$-
508 sensitivity from July–August to June SPEI suggests an earlier impact of drought stress
509 that could slow down cambial activity in peak summer, as already observed in mountain
510 forests of the Alps (Reynolds-Henne *et al*. 2007). Our results expand this observation to
511 low-elevation Mediterranean forests subjected to prolonged summer drought, indicating
512 a coherent but altitude-dependent regional shift in vegetative activity towards more
513 favourable periods (spring).

514 The only relevant climate signals imprinted in $TRW_i$ after removing $\Delta^{13}C_i$-
515 related information were found at high elevation. This observation agrees with the
516 aforementioned sudden weakening of common $TRW_i$ and $\Delta^{13}C_i$ signals found in these
517 forests. Particularly, we observed that increasingly warm winters negatively affected
518 radial growth, likely due to greater cavitation risk during freeze-thaw episodes
519 associated with temperature fluctuations (Peguero-Pina *et al*. 2011). With this
520 exception, most significant correlations between $TRW_i$ and climate disappeared in the
521 1990s after controlling for $\Delta^{13}C_i$, which indicates an intensified climate effect on water
522 conservation strategies underlying regional tree growth. We suppose that other factors
523 potentially related to $TRW_i$ and $\Delta^{13}C_i$ may have influenced these relationships to some
524 extent. Particularly, nutrient effects across the gradient could be differentiated in future
525 studies using a multi-isotopic approach (C, N and O isotopes) (Silva *et al*. 2015),
526 although the study forests are located in a "nutrient-poor" and very depopulated area
527 with low N deposition rates: mean $N\text{-}NH_4^+$ throughfall deposition in a *P. nigra* forest
528 for the region has been estimated as 1.82 kg $ha^{-1}$ $year^{-1}$ during the period 1997–2010,
529 which is in the lowest decile of European records (Waldner *et al*. 2014)

530 An increased severity and duration of drought episodes was recently postulated
531 as a major cause for growth decline in pinewoods within the study area (Camarero *et al*.
532 2015b), with the exception of *P. halepensis* (*cf*. Fig. 6), which tolerates drought better
533 than the other pine species (Matías *et al*. 2016). The increasing trends in $WUE_i$ since
534 1950, together with the lack of growth enhancement for most site-species combinations,
535 suggest that stomatal closure induced by drought has increased $WUE_i$ regionally but at
536 the cost of reduced radial growth. The case of *P. halepensis* may denote an extension of

the actual growing season towards earlier months in winter–early spring boosting growth, but unrelated to $CO_2$ stimulation of photosynthesis.

If we consider the altitudinal gradient of this study as indicative of future climate conditions in the Iberian Peninsula, then we can conclude that Mediterranean mountain pinewoods are becoming more vulnerable to drought as reflected by: (*i*) enhanced spatial synchrony of radial growth owing to more coherent temporal growth patterns among elevation belts, (*ii*) shifting growth sensitivity to water availability towards earlier months in the growing season and (*iii*) increasing dependence of radial growth on stomatal control of water losses spreading upwards in mountain forests, hence resembling lowland forests. Notably, present-day climatic influences on regional tree growth were predominantly related to water conservation strategies, as reflected in wood $\Delta^{13}C$. However, the high-elevation belt exhibited a diverging reaction to warming, showing a sudden uncoupling between leaf-level physiology and growth which deserves further investigation. Altogether, our findings underline the complexities of warming-induced drought effects on Mediterranean forest ecosystems.

## Acknowledgements

T.A.S. and J.P.F acknowledge ERANET-Mundus (European Commission, Grant agreement 20112573) and the Ramón y Cajal program (RYC-2008-02050) respectively. A.A.K. benefitted from a visiting grant (University of Lleida). This study was supported by projects AGL2015-68274-C3-3-R (MINECO/FEDER) and 2014 SGR1141 (Catalan Government). We acknowledge P. Sopeña and M.J. Pau for technical assistance and G. Sangüesa-Barreda for field sampling.

## Data Accessibility

Data are available in Appendix S1, Table S2.

## References

Andreu, L., Gutiérrez, E., Macias, M., Ribas, M., Bosch, O. & Camarero, J.J. (2007) Climate increases regional tree growth variability in Iberian pine forests. *Global Change Biology*, **13**, 1–12.

Andreu, L., Planells, O., Gutiérrez, E., Helle, G. & Schleser, G.H. (2008) Climatic significance of tree-ring width and $\delta^{13}C$ in a Spanish pine forest network. *Tellus B*, **60**, 771–781.

Bunn, A.G., Waggoner, L.A. & Graumlich, L.J. (2005) Topographic mediation of growth in high elevation foxtail pine (*Pinus balfouriana* Grev. et Balf.) forests in the Sierra Nevada, USA. *Global Ecology and Biogeography*, **14**, 103–114.

Camarero, J.J., Gazol, A., Tardif, J.C. & Conciatori, F. (2015a) Attributing forest responses to global-change drivers: limited evidence of a $CO_2$-fertilization effect in Iberian pine growth. *Journal of Biogeography*, **42**, 2220–2233.

Camarero, J.J., Gazol, A., Sangüesa-Barreda, G., Oliva, J. & Vicente-Serrano V. (2015b) To die or not to die: early warnings of tree dieback in response to a severe drought. *Journal of Ecology*, **103**, 44–57.

del Castillo, J., Voltas, J. & Ferrio, J.P. (2015) Carbon isotope discrimination, radial growth, and NDVI share spatiotemporal responses to precipitation in Aleppo pine. *Trees*, **29**, 223–233.

583 Deslauriers, A., Rossi, S., Anfodillo, T. & Saracino, A. (2008) Cambial phenology,
584 wood formation and temperature thresholds in two contrasting years at high
585 altitude in southern Italy. *Tree Physiology*, **28**, 863–871.
586 DeSoto, L., Camarero, J.J., Olano, J.M. & Rozas, V. (2012) Geographically structured
587 and temporally unstable growth responses of *Juniperus thurifera* to recent climate
588 variability in the Iberian Peninsula. *European Journal of Forest Research*, **131**,
589 905–917.
590 FAO (1981) Soil Map of the World. Volume V. Europe. Unesco, Paris.
591 Farquhar, G.D., Ehleringer, J. & Hubick, K. (1989) Carbon isotope discrimination and
592 photosynthesis. *Annual Review of Plant Physiology and Plant Molecular Biology*,
593 **40**, 503–537.
594 Ferrio, J.P., Araus, J.L., Buxó, R., Voltas, J. & Bort, J. (2005) Water management
595 practices and climate in ancient agriculture: inferences from the stable isotope
596 composition of archaeobotanical remains. *Vegetation History and Archaeobotany*,
597 **14**, 510–517.
598 Froux, F., Ducrey, M., Dreyer, E. & Huc, R. (2005) Vulnerability to embolism differs in
599 roots and shoots and among three Mediterranean conifers: consequences for
600 stomatal regulation of water loss? *Trees*, **19**, 137–144.
601 Gagen, M., McCarroll, D. & Edouard, J.L. (2006) Combining tree ring width, density
602 and stable carbon isotope series to enhance the climate signal in tree rings: an
603 example from the French Alps. *Climatic Change*, **78**, 363–379.
604 Galván, J.D., Büntgen, U., Ginzler, C., Grudd, H., Gutiérrez, E., Labuhn, I. *et al*. (2015)
605 Drought-induced weakening of growth-temperature associations in high-elevation
606 Iberian pines. *Global and Planetary Change*, **124**, 95–106.

607 Gessler, A., Ferrio, J.P., Hommel, R., Treydte, K., Werner, R.A. & Monson, R.K.
608 (2014) Stable isotopes in tree rings: towards a mechanistic understanding of
609 isotope fractionation and mixing processes from the leaves to the wood. *Tree*
610 *Physiology*, **34**, 796–818.
611 Gómez-Aparicio, L., García-Valdés, R., Ruíz-Benito, P. & Zavala, M.A. (2011)
612 Disentangling the relative importance of climate, size and competition on tree
613 growth in Iberian forests: implications for forest management under global
614 change. *Global Change Biology*, **17**, 2400–2414.
615 Hartl-Meier, C., Zang, C., Büntgen, U., Esper, J., Rothe, A., Göttlein, A. *et al*. (2014)
616 Uniform climate sensitivity in tree-ring stable isotopes across species and sites in
617 a mid-latitude temperate forest. *Tree Physiology*, **35**, 4–15.
618 Hargreaves, G.H., Samani, Z.A. (1982) Estimating potential evapo-transpiration.
619 *Journal of the Irrigation and Drainage Division*, **108**, 225–230.
620 Haylock, M.R., Hofstra, N., Klein Tank, A.M.G., Klok, E.J., Jones, P.D. & New, M.
621 (2008) A European daily high-resolution gridded dataset of surface temperature
622 and precipitation. *Journal of Geophysical Research*, **113**, D20119.
623 Holmes, R.L. (1983) Computer-assisted quality control in tree-ring dating and
624 measurement. *Tree-Ring Bulletin*, **43**, 69–78.
625 Holzkämper, S., Kuhry, P., Kultti, S., Gunnarson, B. & Sonninen, E. (2008) Stable
626 isotopes in tree rings as proxies for winter precipitation changes in the Russian
627 Arctic over the past 150 years. *Geochronometria*, **32**, 37–46.
628 Hughes, M.K., Kelly, P.M., Pilcher, J.R. & LaMarche, Jr.V.C. (1982) *Climate from tree*
629 *rings*. Cambridge University Press, Cambridge.

630 IPCC (2013) Summary for policymakers. *Climate change 2013: The physical science*
631 *basis. Contribution of Working Group I to the Fifth Assessment Report of the*
632 *Intergovernmental Panel on Climate Change* (ed. by T.F. Stocker, D. Qin, G.-K.
633 Plattner, M. Tignor, S.K. Allen, J. Boschung, A. *et al.*), pp. 3–29. Cambridge
634 University Press, Cambridge.
635 Irvine, J., Perks, P., Magnani, F. & Grace, J. (1998) The response of *Pinus sylvestris* to
636 drought: stomatal control of transpiration and hydraulic conductance. *Tree*
637 *Physiology*, **18**, 393–402.
638 Kienast, F., Schweingruber, F.H., Braker, O.U. & Schar, E. (1987) Tree-ring studies on
639 conifers along ecological gradients and potential of single-year analyses.
640 *Canadian Journal of Forest Research*, **17**, 683–696.
641 Klein, T., Cohen, S., & Yakir, D. (2011) Hydraulic adjustments underlying drought
642 resistance of *Pinus halepensis*. *Tree Physiology*, **31**, 637–648.
643 Klein, T. (2014) The variability of stomatal sensitivity to leaf water potential across tree
644 species indicates a continuum between isohydric and anisohydric behaviours.
645 *Functional Ecology*, **28**, 1313–1320.
646 Leavitt, S.W. (2008) Tree-ring isotopic pooling without regard to mass: No difference
647 from averaging $\delta^{13}C$ values of each tree. *Chemical Geology*, **252**, 52–55.
648 Lévesque, M., Saurer, M., Siegwolf, R., Eilmann, B., Brang, P., Bugmann, H. *et al.*
649 (2013) Drought response of five conifer species under contrasting water
650 availability suggests high vulnerability of Norway spruce and European larch.
651 *Global Change Biology*, **19**, 3184–3199.
652 Livingston, N.J., Whitehead, D., Kelliher, F.M., Wang, Y.P., Grace, J.C., Walcroft, A.S.
653 *et al.* (1998) Nitrogen allocation and carbon isotope fractionation in relation to

intercepted radiation and position in a young *Pinus radiata* D. Don tree. *Plant, Cell & Environment*, **21**, 795–803.

Matías, L., Castro, J., Villar-Salvador, P., Quero, J. & Jump, A.S. (2016) Differential impact of hotter drought on seedling performance of five ecologically distinct pine species. *Plant Ecology*, doi:10.1007/s11258-016-0677-7.

McCarroll, D. & Loader, N.J. (2004) Stable isotopes in tree rings. *Quaternary Science Reviews*, **23**, 771–801.

Natalini, F., Correia, A.C., Vázquez-Piqué, J. & Alejano, R. (2015) Tree rings reflect growth adjustments and enhanced synchrony among sites in Iberian stone pine (*Pinus pinea* L.) under climate change. *Annals of Forest Science*, **72**, 1023–1033.

Pasho, E., Camarero, J.J., de Luis, M. & Vicente-Serrano, S.M. (2011) Impacts of drought at different time scales on forest growth across a wide climatic gradient in north-eastern Spain. *Agricultural and Forest Meteorology*, **151**, 1800–1811.

Peguero-Pina, J.J., Alquézar-Alquézar, J.M., Mayr, S., Cochard, H. & Gil-Pelegrín, E. (2011) Embolism induced by winter drought may be critical for the survival of *Pinus sylvestris* L. near its southern distribution limit. *Annals of Forest Science*, **68**, 565–574.

Picon C., Guehl J.M. & Ferhi A. (1996) Leaf gas exchange and carbon isotope composition responses to drought in a drought-avoiding (*Pinus pinaster*) and a drought-tolerant (*Quercus petraea*) species under present and elevated atmospheric $CO_2$ concentrations. *Plant, Cell & Environment*, **19**, 182–190.

Price, R.A., Liston, A. & Strauss, S.H. (1998) Phylogeny and systematics. *Ecology and Biogeography of Pinus* (ed. by D.M. Richardson), pp. 49–68. Cambridge University Press, Cambridge.

678 Reynolds-Henne, C.E., Siegwolf, R.T.W., Treydte, K.S., Esper, J., Henne, S. & Saurer,
679 M. (2007) Temporal stability of climate-isotope relationships in tree rings of oak
680 and pine (Ticino, Switzerland). *Global Biogeochemical Cycles*, **21**, GB4009.
681 Sánchez-Salguero, R., Camarero, J.J., Hevia, A., Madrigal-González, J., Linares, J.C.,
682 Ballesteros-Canovas, J.A. *et al*. (2015) What drives growth of Scots pine in
683 continental Mediterranean climates: Drought, low temperatures or both?
684 *Agricultural and Forest Meteorology*, **206**, 151–162.
685 Saurer, M., Cherubini, P., Reynolds-Henne, C.E., Treydte, K.S., Anderson, W.T. &
686 Siegwolf, R.T.W. (2008) An investigation of the common signal in tree-ring
687 stable isotope chronologies at temperate sites. *Journal of Geophysical Research*,
688 **113**, G02019.
689 Shestakova, T.A., Aguilera, M., Ferrio, J.P., Gutiérrez, E. & Voltas, J. (2014)
690 Unravelling spatiotemporal tree-ring signals in Mediterranean oaks: a variance-
691 covariance modelling approach of carbon and oxygen isotope ratios. *Tree*
692 *Physiology*, **34**, 819–838.
693 Shestakova, T.A., Gutiérrez, E., Kirdyanov, A.V., Camarero, J.J., Génova, M., Knorre,
694 A.A. *et al*. (2016) Forests synchronize their growth in contrasting Eurasian
695 regions in response to climate warming. *Proceedings of the National Academy of*
696 *Sciences of the United States of America*, **113**, 662–667.
697 Silva, L.C.R., Gómez-Guerrero, A., Doane, T.A. & Horwath, W.R. (2015) Isotopic and
698 nutritional evidence for species- and site-specific responses to N deposition and
699 elevated CO2 in temperate forests. *Journal of Geophysical Research*, **120**, 1110–
700 1123.

701 Tapias, R., Climent, J., Pardos, J.A. & Gil, L. (2004) Life histories of Mediterranean
702 pines. *Plant Ecology*, **171**, 53–68.
703 Vicente-Serrano, S.M., Beguería, S., & López-Moreno, J.I. (2010) A Multi-scalar
704 drought index sensitive to global warming: The Standardized Precipitation
705 Evapotranspiration Index – SPEI. *Journal of Climate*, **23**, 1696–1718.
706 Voltas, J., Camarero, J.J., Carulla, D., Aguilera, M., Ortiz, A. & Ferrio, J.P. (2013) A
707 retrospective, dual-isotope approach reveals individual predispositions to winter-
708 drought induced tree dieback in the southernmost distribution limit of Scots pine.
709 *Plant, Cell & Environment*, **36**, 1435–1448.
710 Voelker, S.L., Meinzer, F.C., Lachenbruch, B., Brooks, J.R. & Guyette, R.P. (2014)
711 Drivers of radial growth and carbon isotope discrimination of bur oak (*Quercus*
712 *macrocarpa* Michx.) across continental gradients in precipitation, vapour pressure
713 deficit and irradiance. *Plant, Cell & Environment*, **37**, 766–779.
714 Waldner, P., Marchetto, A., Thimonier, A., Schmitt, M., Rogora, M., Granke, O. *et al*.
715 (2014) Detection of temporal trends in atmospheric deposition of inorganic
716 nitrogen and sulphate to forests in Europe. *Atmospheric Environment*, **95**, 363–
717 374.
718

## Supporting information captions

Additional Supporting Information can be found in the online version of this article.

**Appendix S1.** Supplementary Materials and Methods and Supplementary Tables S1–S2 and Figures S1–S7.

## Authors′ contribution

T.A.S., E.G. and J.V. conceived and designed the study. J.J.C., A.A.K. and J.V. collected the data. T.A.S. and J.V. carried out the analysis and led the writing, with substantial contributions from J.J.C., A.A.K., J.P.F and E.G. All the authors read and approved the final draft.

731 **Table 1**. Geographical and topographic characteristics of the sampling sites.

732

| Latitude (N) | Longitude (W) | Elevation (m) | Aspect | Geological substrate | Sampled (dominant) species | Other woody species* |
|---|---|---|---|---|---|---|
| ***High-altitude site (HS)*** | | | | | | |
| 40º23'30" | 0º39'50" | 2020 | N-NE | Limestones | *P. sylvestris, P. uncinata* | *Jc, Js, Ra* |
| ***Mid-altitude site (MS)*** | | | | | | |
| 40º19'19" | 0º42'08" | 1615 | SE | Limestones | *P. nigra, P. sylvestris* | *Jc, Jt, Bv, Qi, Ao* |
| ***Low-altitude sites (LS)*** | | | | | | |
| (1) 40º17'17" | 0º48'03" | 1095 | S-SW | Limestones | *P. halepensis* | *Pp, Gs, Jp, Qi* |
| (2) 40º19'45" | 0º48'26" | 1090 | E | Sandstones | *P. nigra, P. pinaster* | *Qf, Qi, Jo, Jp* |

* Species' codes: *Ao, Amelanchier ovalis; Bv, Berberis vulgaris; Gs, Genista scorpius; Jc, Juniperus communis; Jo, J. oxycedrus; Jp, J. phoenicea; Js, J. sabina; Jt, J. thurifera; Pp, Pinus pinaster; Qf, Quercus faginea; Qi, Q. ilex; Ra, Rhamnus alpina*.

733

734

735 **Table 2**. Structural and dendrochronological characteristics of the sampled sites. Abbreviations: DBH, diameter at breast height (1.30 m);
736 *EPS*, Expressed Population Signal; TRW, tree-ring width; $\Delta^{13}C$, carbon isotope discrimination; *Rbar*, mean interseries correlation. The
737 variability of mean values is expressed as standard deviation (±SD). *EPS* and *Rbar* values for $\Delta^{13}C$ chronologies are calculated using a
738 limited number of years (seven) in which individual tree rings were analysed.

| | | | | | | | | TRW (1950–2011) | | $\Delta^{13}C$ (1950–2011) | | |
|---|---|---|---|---|---|---|---|---|---|---|---|---|
| **Tree species** | **Code** | **Basal area ($m^2$ $ha^{-1}$)** | **DBH (cm)** | **Height (m)** | **No. trees (cores)** | **Age at coring height (years)** | **EPS > 0.85 since** | **Mean (mm)** | ***Rbar*** | **Mean (‰)** | **EPS** | ***Rbar*** |
| ***High-elevation site (HS)*** | | | | | | | | | | | | |
| *P. sylvestris* | $Ps_{HS}$ | 36.6 | 43.6 ± 2.0 | 9.3 ± 0.5 | 51 (71) | 116 ± 10 | 1866 | 1.12 ± 0.09 | 0.41 | 17.31 ± 0.22 | 0.82 | 0.48 |
| *P. uncinata* | $Pu_{HS}$ | 36.6 | 39.8 ± 1.7 | 10.4 ± 0.3 | 40 (51) | 100 ± 5 | 1902 | 1.31 ± 0.09 | 0.45 | 17.30 ± 0.21 | 0.74 | 0.36 |
| ***Mid-elevation site (MS)*** | | | | | | | | | | | | |
| *P. nigra* | $Pn_{MS}$ | 38.0 | 46.6 ± 2.7 | 9.9 ± 0.5 | 30 (39) | 131 ± 5 | 1861 | 0.77 ± 0.05 | 0.58 | 17.23 ± 0.20 | 0.82 | 0.47 |
| *P. sylvestris* | $Ps_{MS}$ | 38.0 | 41.0 ± 2.0 | 10.5 ± 1.0 | 31 (40) | 114 ± 8 | 1880 | 1.11 ± 0.12 | 0.53 | 16.44 ± 0.24 | 0.81 | 0.45 |
| ***Low-elevation sites (LS)*** | | | | | | | | | | | | |
| *P. nigra* | $Pn_{LS}$ | 28.0 | 35.6 ± 1.4 | 10.0 ± 0.4 | 37 (54) | 112 ± 6 | 1868 | 0.93 ± 0.13 | 0.60 | 17.25 ± 0.24 | 0.81 | 0.46 |
| *P. pinaster* | $Pp_{LS}$ | 28.0 | 38.8 ± 2.7 | 10.1 ± 0.5 | 33 (49) | 89 ± 3 | 1902 | 1.09 ± 0.14 | 0.67 | 16.97 ± 0.25 | 0.75 | 0.37 |
| *P. halepensis* | $Ph_{LS}$ | 8.2 | 40.0 ± 2.7 | 8.6 ± 0.8 | 32 (48) | 75 ± 3 | 1915 | 1.68 ± 0.09 | 0.67 | 16.85 ± 0.34 | 0.94 | 0.76 |

739

740 FIGURE CAPTIONS

741

742 **Figure 1**. Regional temporal trends in climate data for the study area (period 1950–
743 2011). (a) Annual and (b) monthly long-term changes in mean temperature (top),
744 precipitation (middle) and difference between precipitation and potential
745 evapotranspiration (P-PET) (bottom) derived from the European high-resolution climate
746 dataset (E-OBS). Annual E-OBS trends (black lines) are smoothed by LOESS fitting
747 (span = 0.5). Bars represent slopes of linear regressions of monthly climate factors as a
748 function of time. Filled bars indicate significant linear trends over time ($P \leq 0.05$).

749

750 **Figure 2**. Principal component analysis (a) and synchrony patterns (b) along the
751 altitudinal gradient. All calculations are based on indexed tree-ring width ($TRW_i$)
752 chronologies. The plot of the first and second principal components (PC1 and PC2,
753 respectively) shows the loadings of each chronology for the common period 1950–
754 2011. Temporal trends in spatial synchrony are estimated for 50-year periods lagged by
755 five years for all chronologies ($\hat{a}_C$) (eqn 6, Appendix S1) and for pairs of chronologies
756 belonging to different altitudinal belts ($\hat{a}_{Cb}$) (eqn 7, Appendix S1). Significant linear
757 trends of $\hat{a}_C$ and $\hat{a}_{Cb}$ values over time are depicted as straight lines ($P < 0.05$). Shaded
758 areas indicate standard errors.

759

760 **Figure 3**. Temporal trends in intra-site associations between $TRW_i$ and $\Delta^{13}C_i$
761 chronologies along the altitudinal gradient. The correlations of year effects ($r_Y$) are
762 estimated for 25-year periods lagged by one year following eqn (eqn 2) in Materials and
763 Methods. The standard error (SE) of $r_Y$ (shaded areas) is used to compute the sampling

764 distribution (95%) of the actual correlation value (±2SE). Significant correlations
765 (correlation coefficients with confidence intervals not embracing zero) are depicted as
766 filled dots.
767
768 **Figure 4**. Altitudinal changes in $TRW_i$ (a) and $\Delta^{13}C_i$ (b) responses to climate. Tree-ring
769 trait relationships with climate are based on Pearson correlations between the master
770 chronology corresponding to each altitudinal belt and monthly mean temperature,
771 precipitation and the SPEI drought index (calculated at one-, three- and six-month
772 scales) for the period 1950–2011. The horizontal lines indicate the threshold for
773 significance (dashed line, $P < 0.05$; dotted line, $P < 0.01$). Lowercase and uppercase
774 letters in the *x*-axes correspond to months of the years before and during tree-ring
775 formation, respectively.
776
777 **Figure 5**. Moving correlations between the master $TRW_i$ and $\Delta^{13}C_i$ chronologies of
778 each altitudinal belt and monthly mean temperature (a) and one-month drought index
779 SPEI1 (b) (period 1950–2011). The threshold for significance is $r = \pm 0.37$ ($n = 25$ years;
780 $P < 0.05$). Non-filled areas denote non-significant correlations. Lowercase and
781 uppercase letters in the *y*-axes correspond to months of the years before and during tree-
782 ring formation, respectively.
783
784 **Figure 6.** Temporal trends in intrinsic water-use efficiency ($WUE_i$) and basal area
785 increment (BAI) and relationships between them for every site-species combination for
786 the period 1950–2011. (a) Observed temporal trends in $WUE_i$ (solid colored lines) as
787 related to a theoretical model assuming a constant ratio between intercellular and

788 atmospheric $CO_2$ concentrations ($C_i/C_a$ = ctn scenario; dashed colored lines), which
789 fitted better the experimental data (Appendix S1). Blue lines refer to the high-elevation
790 site (HS), green lines to the mid-elevation site (MS) and red lines to the low-elevation
791 sites (LS). Grey lines denote corresponding temporal changes in mean BAI. Significant
792 linear trends of BAI over time are depicted as straight lines. (b) Relationships between
793 $WUE_i$ and BAI. Significant linear associations are depicted as black lines (*: $P < 0.05$;
794 **: $P < 0.01$; ***: $P < 0.001$).

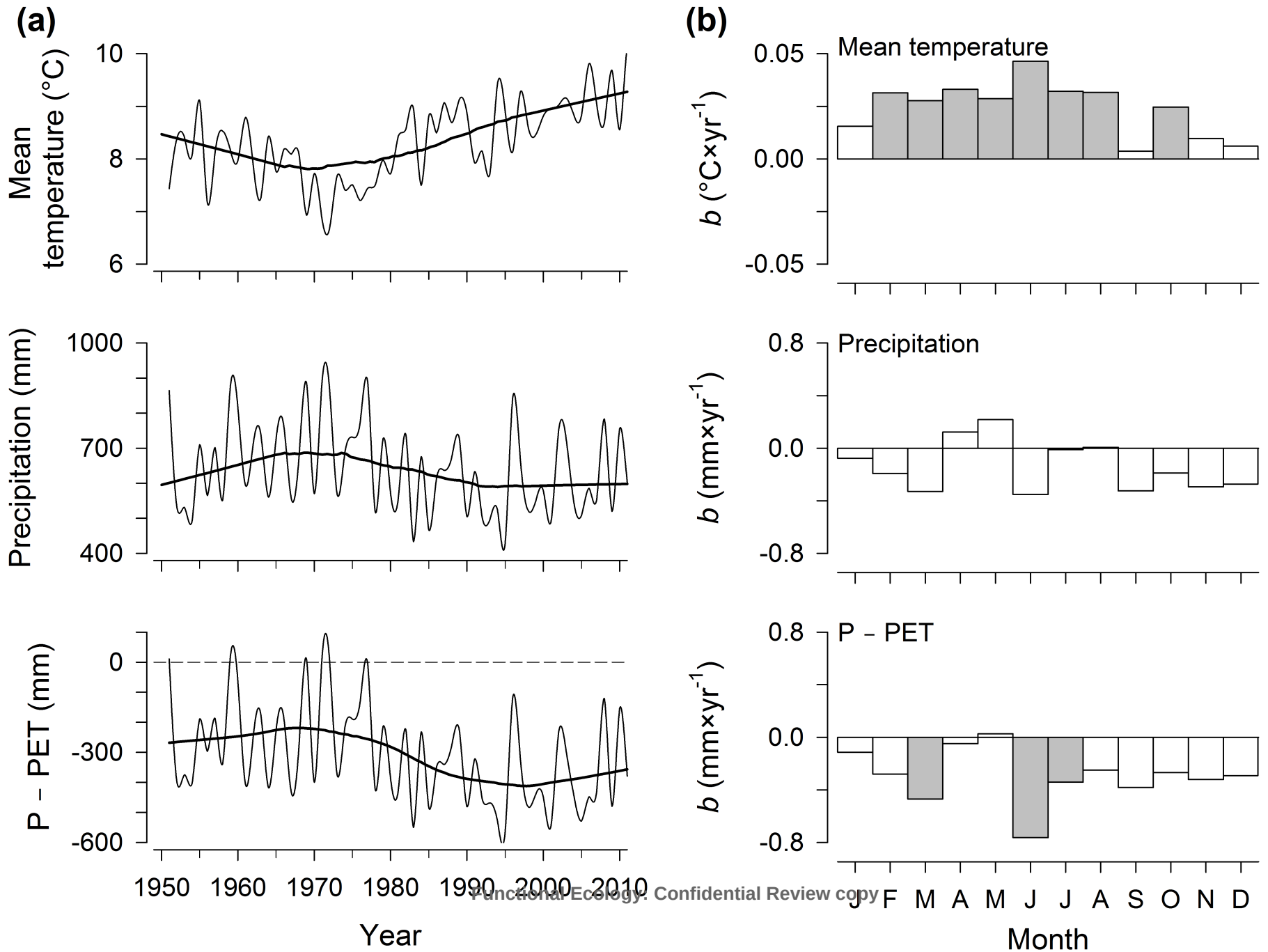

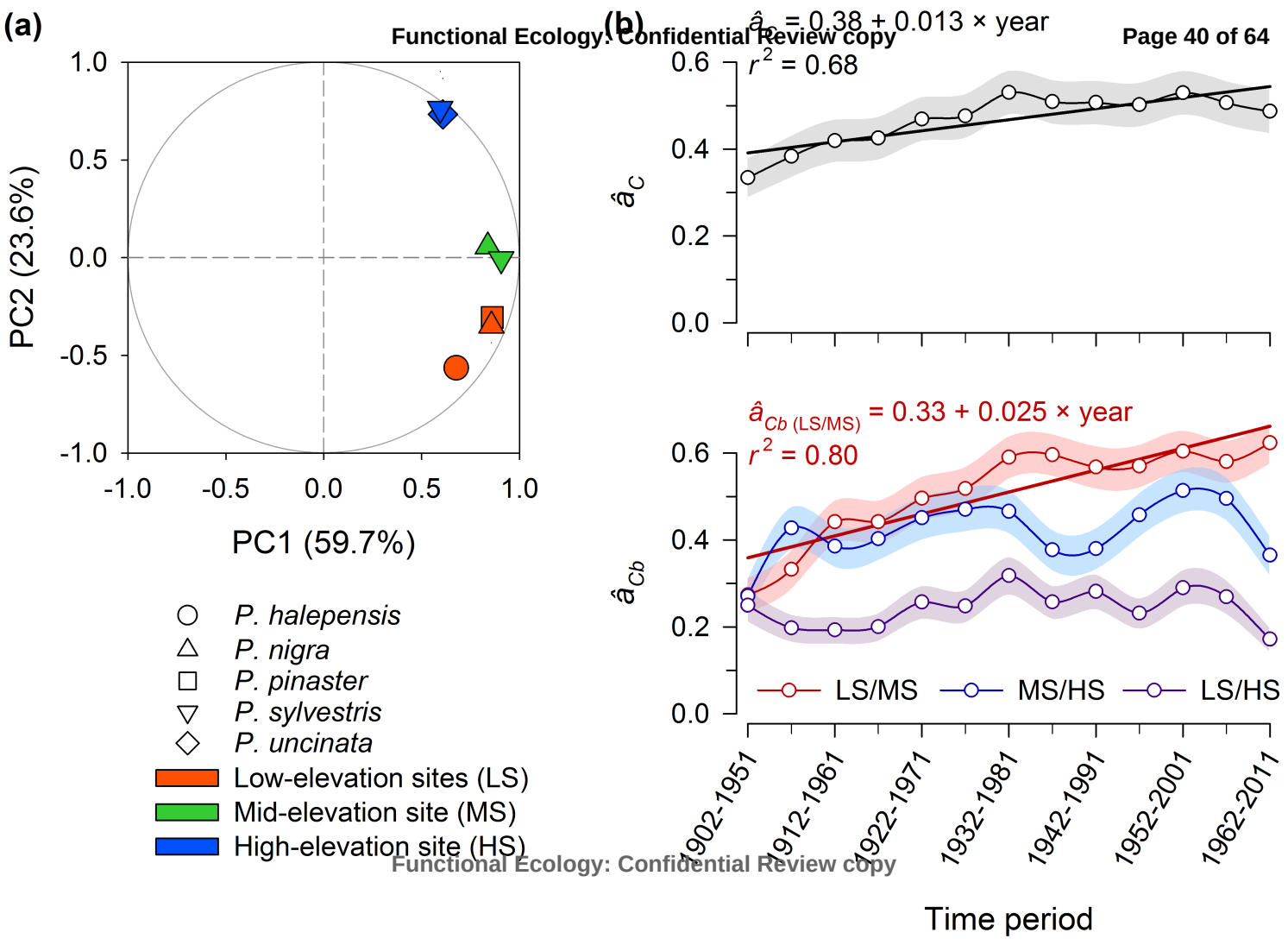

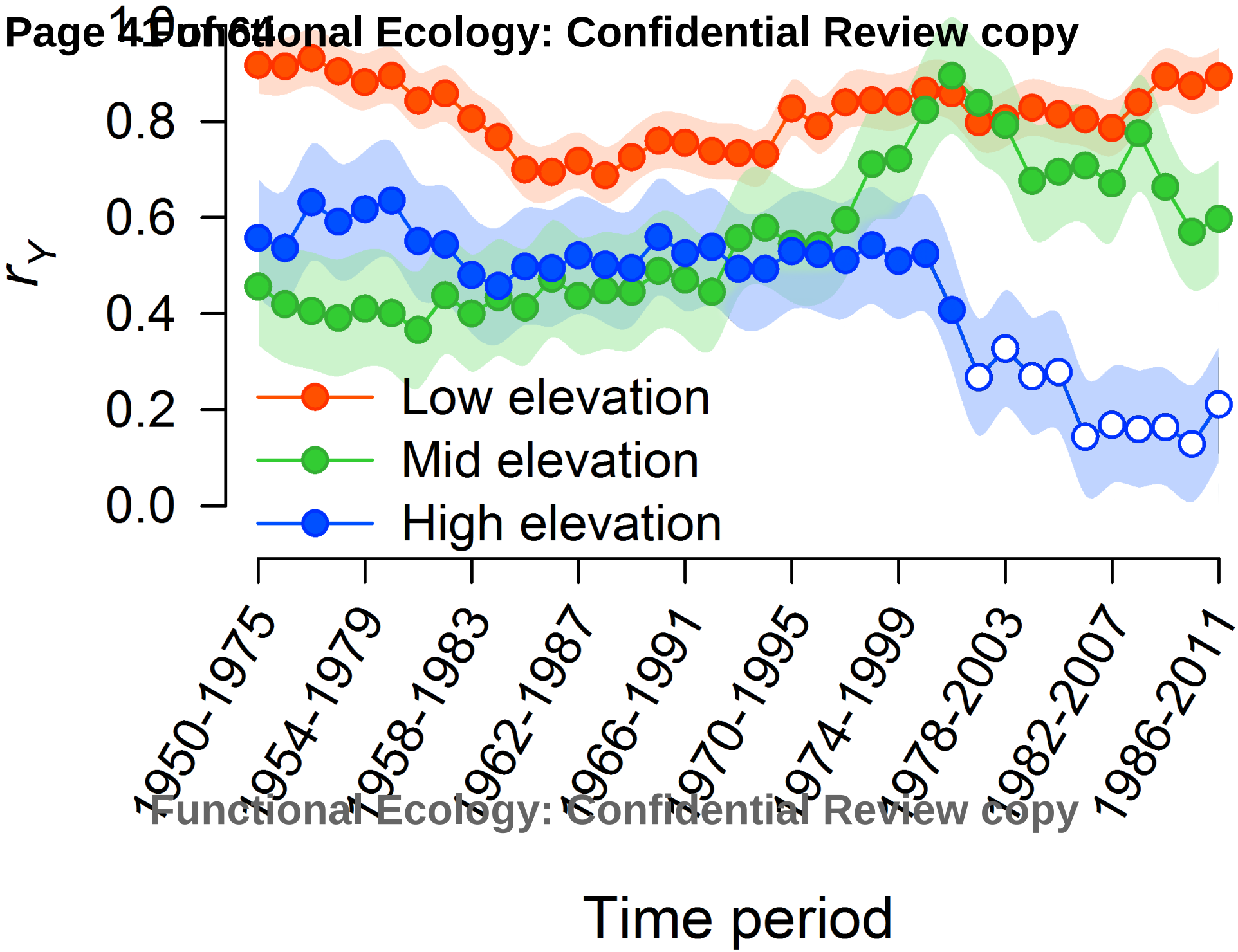

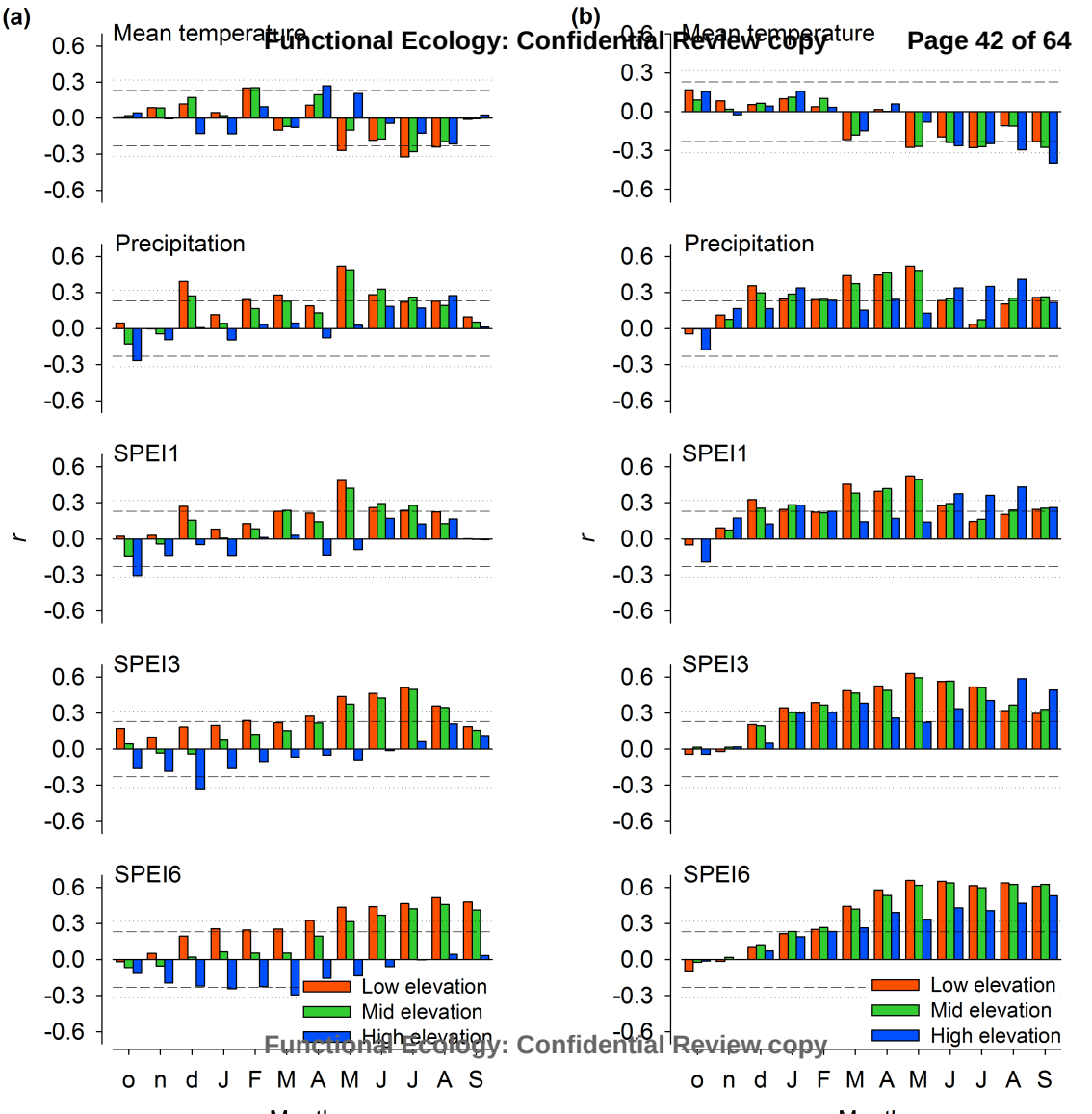

(a) Mean temperature - $TRW_i$

Mean temperature - $\Delta^{13}C_i$

(b) SPEI1 - $TRW_i$

SPEI1 - $\Delta^{13}C_i$

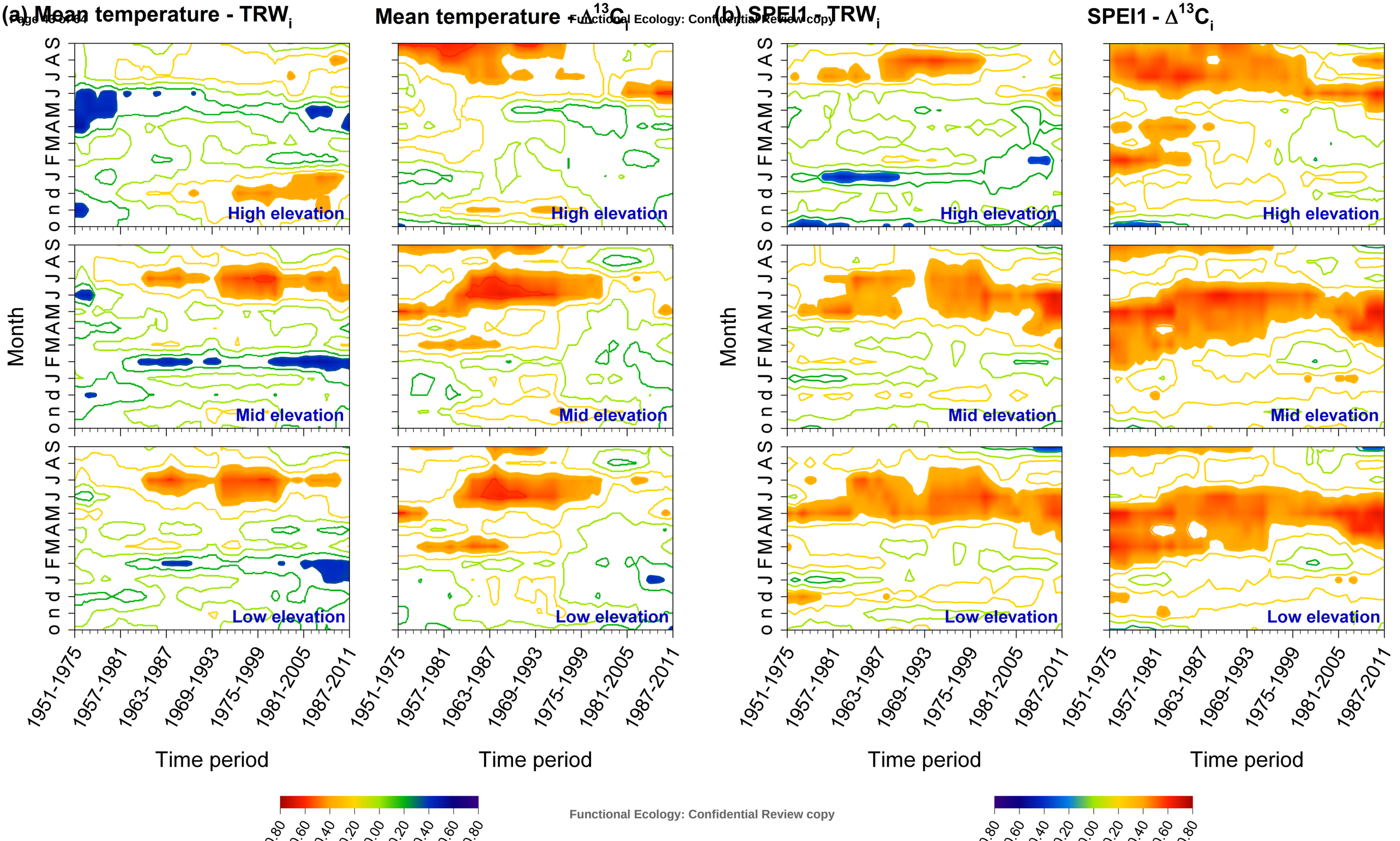

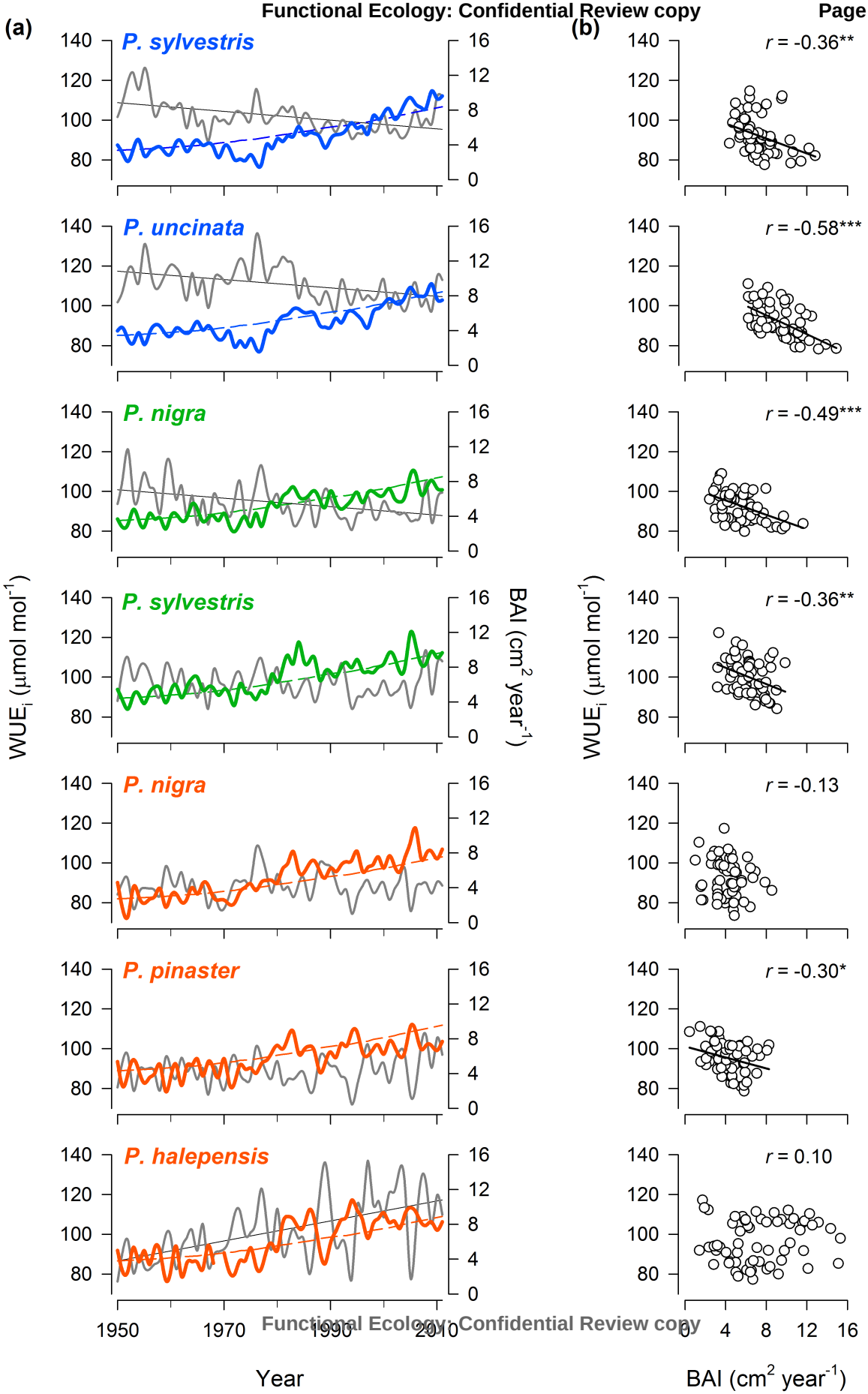

*Functional Ecology*

**SUPPORTING INFORMATION**

# Increasing drought effects on five European pines modulate $\Delta^{13}C$-growth coupling along a Mediterranean altitudinal gradient

T.A. Shestakova, J.J. Camarero, J.P. Ferrio, A.A. Knorre, E. Gutiérrez, J. Voltas

**Appendix S1:** *Supplementary Materials and Methods and Supplementary Tables S1–S2 and Figures S1–S7*

**Table of Contents**

**Supplementary details on climate analysis**

*Meteorological data and climate gradients*

In general, climate estimates obtained from the European high-resolution climate dataset (E-OBS; Haylock *et al.* 2008) can be considered of reasonable quality (Herrera *et al.* 2010). Here we compared the E-OBS series with local records from the closest weather station, situated approximately 40 km west (Teruel, 40°21'N, 1°07'W, 900 m a.s.l.). The correlations between gridded and station data were high ($r = 0.92$, $P < 0.001$ and $r = 0.78$, $P < 0.001$, for mean annual temperature and precipitation, respectively, during the common period 1986–2011), suggesting that the E-OBS dataset is representative of the regional climate.

Further, to estimate the range of climatic variation between altitudinal extremes we applied lapse rate adjustments to the E-OBS dataset as follows (Gandullo 1994): for temperature, decrease in 0.6°C per 100 m; for precipitation, 8% increment per 100 m, except for July and August, when precipitation is unrelated to altitude (Fig. S2).

**Supplementary details on dendrochronological methods**

*Development of tree-ring width and $\Delta^{13}$C chronologies and BAI calculation*

In order to build indexed tree-ring width ($TRW_i$) chronologies for each site and species, the individual series were first standardised using a cubic-smoothing spline curve of 100 years with a 50%-frequency response cut-off. This procedure minimizes the influence of biological trends (e.g. tree age and size) and disturbance effects (e.g. due to forest management) on radial growth, hence preserving high-frequency variability potentially related to climate. Thus, standardisation converted ring-width measurements into dimensionless indices with mean value of 1. This standardisation procedure was complemented with a sensitivity analysis to assess the influence of detrending spline rigidity on the ring-width indices as some sampled trees were relatively young (i.e. <150 years). This means that a spline curve of 100 years could remove less of the variation owing to stand dynamics from the young growth stages compared to older growth stages, hence affecting synchrony estimates as presented in Fig. 2b of main document. To this end, we tested for the effect of cubic smoothing splines of different lengths (50 years, 30 years, and 15 years) on growth synchrony trends (see Supplementary details on statistical analysis of this Appendix).

Next, autoregressive models were applied to remove the first-order temporal autocorrelation in the detrended series and generate residual or pre-whitened indices. Finally, a biweight robust mean was computed to produce indexed chronologies for each site and species and for every cubic smoothing spline tested. Results of the default method (spline of length = 100 years) are shown in Fig. 2b. These procedures were done using the ARSTAN program (Cook & Krusic 2005). The reliability of ring-width chronologies for capturing the hypothetical population signal was checked against the expressed population signal (*EPS*) criterion with a threshold value of 0.85 (Wigley, Briffa & Jones 1984). Interseries correlation (*Rbar*) statistics were used to estimate the internal coherence of each chronology (Wigley *et al.* 1984). These parameters are shown in Table 2 of main document.

In the case of $\Delta^{13}$C, mean yearly values per species and site were also standardised using a cubic-smoothing spline curve of 100 years with a 50%-frequency response cut-off. This procedure converted $\Delta^{13}$C records into dimensionless indices with mean value of 1. Next, autoregressive models were applied to remove the first-order temporal autocorrelation in the detrended series and generate residual or pre-whitened indices (referred to as $\Delta^{13}C_i$ chronologies in main text). The calculation of a

biweight robust mean could be saved here as mean yearly $\Delta^{13}$C values were used for obtaining each $\Delta^{13}C_i$ chronology. On the other hand, the estimation of between-tree variability in the original $\Delta^{13}$C records (with data available every ten years for estimating tree effects) was carried out by analysis of variance at the chronology level allowing for random year and fixed tree effects. For those years consisting of pooled rings an artificial tree was coded in the dataset so as to obtain standard errors of $\Delta^{13}$C for every year of the study period (1950–2011).

The annual basal area increment (BAI) was calculated from tree-ring series according to:

$$BAI = \pi(R_t^2 - R_{t-1}^2) \quad \text{(eqn 1)}$$

where $R$ is the radius of the tree and $t$ is the year of tree-ring formation.

**Supplementary details on water-use efficiency analysis**

*Estimation of water-use efficiency from $\Delta^{13}C$*

Using $\Delta^{13}$C data, intrinsic water-use efficiency ($WUE_i$) and intercellular $CO_2$ concentration ($C_i$) values were estimated according to:

$$WUE_i = (C_a \times (b - \Delta^{13}C)) / [1.6 \times (b - a)] \quad \text{(eqn 2)}$$

and

$$C_i = [(\Delta^{13}C - a) \times C_a] / (b - a) \quad \text{(eqn 3)}$$

where $C_a$ represents the atmospheric $CO_2$ concentration, $a$ is the fractioning during diffusion through stomata (~4.4‰) and $b$ is the fractioning during carboxylation by Rubisco and PEP carboxylase (~27‰) (Farquhar *et al*. 1989). The factor 1.6 denotes the ratio of diffusivities of water vapour and $CO_2$ in the air. $C_a$ values were taken from the National Oceanic and Atmospheric Administration (NOAA) Earth System Research Laboratory (http://www.esrl.noaa.gov/).

Theoretical $WUE_i$ values were calculated according to three scenarios as proposed by Saurer et al. (2004). These scenarios describe how the $C_i$ might follow the $C_a$ increase over time: (*i*) either not at all, when $C_i$ is maintained constant; (*ii*) in a proportional way, when $C_i/C_a$ is maintained constant; or (*iii*) at the same rate, when $C_a - C_i$ is maintained constant. Initial $C_i$ values were obtained for each site-species combination by applying eqn (eqn 3) to the average $\Delta^{13}$C and $C_a$ values of the first five years of the study period (1950–1954). We used these scenarios to obtain theoretical $WUE_i$ values that were compared to $WUE_i$ records obtained from measured $\Delta^{13}$C. To this end, the sum of squared differences between actual and predicted $WUE_i$ values (according to the different scenarios) was divided by the number of observations (years). The square root of this quantity is the root mean square predictive difference ($RMS_{PD}$), for which smaller values indicated more accurate theoretical predictions (data not shown). For each site-species combination, an increase in $WUE_i$ since the 1950s closely followed a constant $C_i/C_a$ scenario (Fig. 6a).

**Supplementary details on statistical analysis**

*Long-term trends in indexed tree-ring width patterns*

To investigate spatial synchrony patterns in $TRW_i$, we used variance-covariance (VCOV) modelling. First, we calculated the degree to which the complete set of indexed ring-width chronologies ($i$ = 1 to 7) contained a common temporal signal. Briefly, suppose that $W_{ij}$ is the $j$th year of indexed ring-width $W_i$. The estimators can be defined in terms of the following random linear model (random variables are shown underlined in this paper):

$$\underline{W}_{ij} = \underline{Y}_j + \underline{e}_{ij} \quad \text{(eqn 4)}$$

where $Y_j$ is a random time effect of the $j$th year and $e_{ij}$ is a random deviation of the $i$th chronology in the $j$th year. Here, we assume that the year effects behave as if they came from a normal distribution with mean zero and variance $\sigma_Y^2$. The reproducibility of observations by the set of $I$ chronologies can be estimated as (Shestakova *et al*. 2014):

$$\hat{a}_C = \frac{\sigma_Y^2}{\sigma_Y^2 + \sigma_e^2} \quad \text{(eqn 5)}$$

We will refer to $\hat{a}_C$ as the mean interchronology correlation or growth synchrony among chronologies.

Next, the seven chronologies were grouped into potentially homogeneous subsets aimed at investigating synchrony patterns along the altitudinal gradient. Groups of chronologies with similar growth patterns were defined through principal component analysis (PCA) for the common period 1950–2011 (Fig. 2a of main document). To analyse temporal patterns in synchrony within and between groups with distinct growth signals, corresponding to the three altitudinal belts ($r$ = 1 to 3; for details see Results section), the following variance-covariance (VCOV) structure underlying model (eqn 4) was employed (Shestakova *et al.* 2014):

$\text{cov}(\underline{Y}_{jr};\underline{Y}_{jr^*}) = \sigma_{Y_r}^2$, when $r = r^*$,

otherwise $\text{cov}(\underline{Y}_{jr};\underline{Y}_{jr^*}) = \sigma_{Y_{rr^*}}^2$

This structure allows each group to have its own year variance and each pair of groups its own year covariance. The mean correlation (synchrony) estimated between all possible pairs of chronologies as in eqn (eqn 5) may be split into (*i*) a mean correlation between pairs of chronologies within every group $r$ ($\hat{a}_{Cw}$) and (*ii*) a mean

correlation between pairs of chronologies belonging to groups *r* and $r^*$ ($\hat{a}_{Cb}$), as follows (Shestakova *et al*. 2014):

$$\hat{a}_{Cw} = \frac{\sigma^2_{Y_r}}{\sigma^2_{Y_r} + \sigma^2_e} \quad \text{(eqn 6)}$$

$$\hat{a}_{Cb} = \frac{\sigma^2_{Y_{rr^*}}}{\sqrt{(\sigma^2_{Y_r} + \sigma^2_e) \times (\sigma^2_{Y_{r^*}} + \sigma^2_e)}} \quad \text{(eqn 7)}$$

In turn, the residual variance $\sigma^2_e$ may vary among groups, hence producing a heteroscedastic variant of the group-based model.

These models (general and group-based heteroscedastic) were tested for 50-year segments lagged by five years for the period 1902–2011. To this end, we used indexed chronologies obtained from different cubic smoothing splines (length = 100 years, 50 years, 30 years and 15 years), hence obtaining separate synchrony trends testing for the influence of detrending spline rigidity. The results for the default method (spline of length = 100 years) are shown in Fig. 2b of main document. The sensitivity analysis illustrating the effect of different splines in growth synchrony trends over time is shown in Fig. S5.

*Relationships between $TRW_i$ and $\Delta^{13}C_i$*

Frequently, two or more features (ring-width, stable isotopes, wood density, etc.) are simultaneously measured on tree rings aiming at understanding changes in tree performance over time. As these features are a consequence of a number of common plant processes (carbon uptake and storage, water use, etc.) they may contain partially overlapping information. To quantify the association between traits, the Pearson product-moment correlation coefficient applied to the time series of *J* years can be used. This approach is valid for observations obtained annually either in the same tree or in the same chronology (i.e. a composite of individual trees). However, there may be an interest to estimate the overall association between traits for a number of trees (or chronologies) simultaneously. A possible approach consists in calculating the Pearson correlation for pairs of observations across years and trees (or chronologies). If so, this correlation contains three different causes of association: temporal (due to year effects), spatial (due to mean differences among trees [chronologies]) and residual (quantifying the specificity of temporal variability at the tree [chronology] level). The temporal association (or correlation of year effects) represents how similarly two traits covariate

across years, while the residual association quantifies how consistent the interaction between time and tree (chronology) effects is across traits. It must be noted that the spatial association is usually obscured in dendrochronology as time-series (trees or chronologies) are usually detrended or indexed prior to the calculation of Pearson correlations, meaning that they take essentially the same mean value.

In this context, the single trait random model (eqn 4) can be extended in order to take into account simultaneously the information available on two different features, thus resulting in a bivariate analysis (White & Hodge 1989). This allows for a straightforward estimation of the temporal association between pairs of traits (i.e. $TRW_i$ and $\Delta^{13}C_i$). Similarly to the calculation of a Pearson correlation (or the covariance between traits divided by the product of their standard deviations), the temporal and residual associations (i.e. correlations) can be estimated by the partition of the general covariance between traits across years and trees (chronologies) in its year and residual components. In this way, the correlation of year effects ($r_Y$) can be expressed as (Gilmour *et al*. 2002):

$$r_Y = \frac{\sigma_{Y_{12}}}{\sqrt{\sigma^2_{Y_1} \times \sigma^2_{Y_2}}} \qquad \text{(eqn 8)}$$

where $\sigma_{Y_{12}}$ is the common variability of year effects underlying traits 1 and 2 (covariance), $\sigma^2_{Y_1}$ stands for the variance component estimate of year effects for trait 1 and $\sigma^2_{Y_2}$ stands for the variance component estimate of year effects for trait 2.

The statistical analyses were performed with SAS/STAT (ver. 9.4, SAS Inc., Cary, NC, USA). We used the MIXED procedure for random modelling and estimation of variance components through restricted maximum likelihood (REML). The covariance structure for groups was specified using the RANDOM statement. Heterogeneity of residual variances across groups was implemented with the GROUP option of the REPEATED statement.

**Supplementary Tables**

**Table S1.** Pearson correlation coefficients between tree-ring traits for the period 1950–2011. Values above the main diagonal are correlations between pairs of indexed tree-ring width ($TRW_i$) chronologies; values below the main diagonal are correlations between pairs of indexed carbon isotope discrimination ($\Delta^{13}C_i$) chronologies. Values in the main diagonal (in bold) are correlations between $TRW_i$ and $\Delta^{13}C_i$ chronologies of the same site and species. Non-significant correlation coefficients ($P \geq 0.05$) are indicated in italics. Chronology codes are as in Table 2 of main document.

| $\Delta^{13}C_i$ \ $TRW_i$ | ***Ps*$_{HS}$** | ***Pu*$_{HS}$** | ***Pn*$_{MS}$** | ***Ps*$_{MS}$** | ***Pn*$_{LS}$** | ***Pp*$_{LS}$** | ***Ph*$_{LS}$** |
|---|---|---|---|---|---|---|---|
| ***Ps*$_{HS}$** | **0.18** | 0.76 | 0.37 | 0.38 | 0.30 | 0.30 | 0.39 |
| ***Pu*$_{HS}$** | 0.91 | **0.43** | 0.35 | 0.48 | 0.30 | 0.35 | 0.41 |
| ***Pn*$_{MS}$** | 0.47 | 0.48 | **0.28** | 0.82 | 0.63 | 0.63 | 0.44 |
| ***Ps*$_{MS}$** | 0.48 | 0.49 | 0.61 | **0.46** | 0.57 | 0.64 | 0.50 |
| ***Pn*$_{LS}$** | 0.28 | 0.27 | 0.58 | 0.74 | **0.48** | 0.87 | 0.59 |
| ***Pp*$_{LS}$** | 0.31 | 0.31 | 0.60 | 0.72 | 0.70 | **0.67** | 0.71 |
| ***Ph*$_{LS}$** | *0.00* | *0.08* | 0.50 | 0.53 | 0.71 | 0.69 | **0.71** |

**Table S2.** Indexed tree-ring width ($TRW_i$) and carbon isotope discrimination ($\Delta^{13}C_i$) chronologies for every site-species combination.

| | $TRW_i$ | | | | | | | $\Delta^{13}C_i$ | | | | | | |
|---|---|---|---|---|---|---|---|---|---|---|---|---|---|---|
| **Year** | ***Ps*$_{HS}$** | ***Pu*$_{HS}$** | ***Pn*$_{MS}$** | ***Ps*$_{MS}$** | ***Pn*$_{LS}$** | ***Pp*$_{LS}$** | ***Ph*$_{LS}$** | ***Ps*$_{HS}$** | ***Pu*$_{HS}$** | ***Pn*$_{MS}$** | ***Ps*$_{MS}$** | ***Pn*$_{LS}$** | ***Pp*$_{LS}$** | ***Ph*$_{LS}$** |
| 1850 | 1.30 | | | | | | | | | | | | | |
| 1851 | 1.00 | | | | | | | | | | | | | |
| 1852 | 0.94 | | | | | | | | | | | | | |
| 1853 | 0.98 | | | | | | | | | | | | | |
| 1854 | 1.19 | | | | | | | | | | | | | |
| 1855 | 0.66 | | | | | | | | | | | | | |
| 1856 | 0.74 | | | | | | | | | | | | | |
| 1857 | 1.04 | | | | | | | | | | | | | |
| 1858 | 0.96 | | | | | | | | | | | | | |
| 1859 | 1.12 | | | | | | | | | | | | | |
| 1860 | 0.97 | | | | | | | | | | | | | |
| 1861 | 0.86 | | 0.93 | | | | | | | | | | | |
| 1862 | 1.10 | | 1.19 | | | | | | | | | | | |
| 1863 | 1.09 | | 1.32 | | | | | | | | | | | |
| 1864 | 1.61 | | 1.02 | | | | | | | | | | | |
| 1865 | 1.30 | | 1.41 | | | | | | | | | | | |
| 1866 | 0.87 | | 1.09 | | | | | | | | | | | |
| 1867 | 0.66 | | 0.48 | | | | | | | | | | | |
| 1868 | 1.08 | | 1.11 | | 1.11 | | | | | | | | | |
| 1869 | 0.90 | | 0.79 | | 0.78 | | | | | | | | | |
| 1870 | 1.06 | | 0.87 | | 0.50 | | | | | | | | | |
| 1871 | 0.99 | | 0.94 | | 1.01 | | | | | | | | | |
| 1872 | 0.93 | | 1.41 | | 1.06 | | | | | | | | | |
| 1873 | 0.81 | | 0.85 | | 1.04 | | | | | | | | | |
| 1874 | 0.86 | | 1.03 | | 0.81 | | | | | | | | | |
| 1875 | 0.99 | | 1.13 | | 0.92 | | | | | | | | | |
| 1876 | 0.82 | | 0.97 | | 0.63 | | | | | | | | | |
| 1877 | 1.18 | | 0.99 | | 0.89 | | | | | | | | | |
| 1878 | 1.11 | | 1.06 | | 1.02 | | | | | | | | | |
| 1879 | 0.42 | | 0.29 | | 0.52 | | | | | | | | | |
| 1880 | 1.03 | | 1.02 | 1.03 | 1.36 | | | | | | | | | |
| 1881 | 0.69 | | 0.68 | 0.78 | 0.56 | | | | | | | | | |
| 1882 | 1.13 | | 0.70 | 0.98 | 1.06 | | | | | | | | | |
| 1883 | 0.88 | | 0.85 | 0.98 | 0.96 | | | | | | | | | |
| 1884 | 1.23 | | 1.36 | 1.15 | 1.33 | | | | | | | | | |
| 1885 | 1.09 | | 1.37 | 1.06 | 0.84 | | | | | | | | | |
| 1886 | 1.09 | | 1.11 | 1.04 | 1.09 | | | | | | | | | |
| 1887 | 0.97 | | 0.69 | 0.86 | 0.92 | | | | | | | | | |
| 1888 | 0.75 | | 1.16 | 1.36 | 1.17 | | | | | | | | | |
| 1889 | 0.90 | | 1.13 | 1.28 | 1.26 | | | | | | | | | |
| 1890 | 0.85 | | 0.91 | 1.13 | 1.04 | | | | | | | | | |
| 1891 | 0.85 | | 1.02 | 1.30 | 1.02 | | | | | | | | | |
| 1892 | 1.27 | | 1.25 | 1.28 | 1.26 | | | | | | | | | |
| 1893 | 1.05 | | 1.08 | 1.10 | 1.15 | | | | | | | | | |
| 1894 | 0.98 | | 1.06 | 1.07 | 0.88 | | | | | | | | | |
| 1895 | 1.09 | | 1.03 | 1.03 | 0.53 | | | | | | | | | |
| 1896 | 0.76 | | 1.19 | 1.11 | 0.99 | | | | | | | | | |
| 1897 | 1.08 | | 1.22 | 1.30 | 0.88 | | | | | | | | | |
| 1898 | 1.06 | | 0.71 | 0.86 | 0.59 | | | | | | | | | |
| 1899 | 0.96 | | 1.00 | 1.14 | 0.82 | | | | | | | | | |
| 1900 | 0.89 | | 0.81 | 0.97 | 1.05 | | | | | | | | | |
| 1901 | 1.09 | | 0.76 | 0.91 | 1.31 | | | | | | | | | |

| | | | | | | | | | | | | | | |
|---|---|---|---|---|---|---|---|---|---|---|---|---|---|---|
| 1902 | 0.93 | 1.00 | 0.76 | 1.01 | 1.23 | 1.13 | | | | | | | | |
| 1903 | 1.08 | 1.03 | 0.81 | 1.11 | 1.05 | 0.97 | | | | | | | | |
| 1904 | 1.12 | 0.99 | 0.73 | 0.74 | 1.24 | 0.99 | | | | | | | | |
| 1905 | 1.33 | 1.22 | 0.51 | 0.87 | 1.09 | 0.97 | | | | | | | | |
| 1906 | 1.06 | 0.99 | 0.86 | 0.97 | 1.02 | 1.04 | | | | | | | | |
| 1907 | 0.99 | 1.03 | 0.77 | 0.83 | 1.06 | 0.84 | | | | | | | | |
| 1908 | 1.07 | 1.05 | 1.15 | 1.06 | 1.46 | 1.11 | | | | | | | | |
| 1909 | 0.80 | 0.86 | 0.88 | 0.90 | 0.96 | 0.73 | | | | | | | | |
| 1910 | 0.74 | 0.77 | 0.78 | 0.81 | 0.95 | 0.87 | | | | | | | | |
| 1911 | 1.06 | 1.05 | 1.26 | 1.26 | 0.43 | 0.90 | | | | | | | | |
| 1912 | 1.10 | 1.16 | 0.79 | 0.72 | 0.59 | 0.88 | | | | | | | | |
| 1913 | 1.12 | 1.09 | 0.84 | 0.81 | 0.86 | 0.93 | | | | | | | | |
| 1914 | 1.23 | 1.21 | 1.57 | 1.26 | 0.89 | 1.14 | | | | | | | | |
| 1915 | 1.16 | 1.15 | 1.17 | 1.11 | 1.17 | 1.50 | 1.04 | | | | | | | |
| 1916 | 0.74 | 0.72 | 0.64 | 0.65 | 0.63 | 0.76 | 0.99 | | | | | | | |
| 1917 | 1.11 | 1.16 | 1.05 | 1.05 | 1.29 | 1.50 | 1.09 | | | | | | | |
| 1918 | 0.84 | 0.87 | 0.74 | 0.75 | 0.99 | 0.76 | 1.10 | | | | | | | |
| 1919 | 1.03 | 1.09 | 1.06 | 0.94 | 1.34 | 1.49 | 0.91 | | | | | | | |
| 1920 | 1.17 | 1.26 | 0.98 | 0.85 | 1.34 | 1.08 | 1.23 | | | | | | | |
| 1921 | 0.83 | 0.87 | 0.87 | 0.97 | 1.25 | 1.26 | 1.27 | | | | | | | |
| 1922 | 0.98 | 1.02 | 1.02 | 0.98 | 1.29 | 1.19 | 1.18 | | | | | | | |
| 1923 | 1.08 | 1.07 | 1.41 | 1.12 | 0.37 | 0.90 | 1.10 | | | | | | | |
| 1924 | 0.89 | 0.89 | 0.66 | 0.69 | 0.54 | 0.83 | 0.97 | | | | | | | |
| 1925 | 1.05 | 0.99 | 1.08 | 1.09 | 0.84 | 1.10 | 0.94 | | | | | | | |
| 1926 | 1.04 | 1.08 | 1.19 | 1.00 | 1.28 | 1.42 | 0.84 | | | | | | | |
| 1927 | 1.05 | 1.11 | 1.04 | 1.17 | 1.23 | 1.25 | 0.98 | | | | | | | |
| 1928 | 0.92 | 0.90 | 0.78 | 0.79 | 0.81 | 0.97 | 0.98 | | | | | | | |
| 1929 | 1.12 | 1.14 | 1.11 | 1.08 | 0.77 | 1.13 | 1.04 | | | | | | | |
| 1930 | 1.05 | 0.95 | 1.20 | 1.07 | 1.16 | 1.08 | 1.12 | | | | | | | |
| 1931 | 0.65 | 0.64 | 0.49 | 0.51 | 0.62 | 0.49 | 0.84 | | | | | | | |
| 1932 | 1.18 | 1.24 | 1.14 | 1.21 | 1.06 | 1.18 | 0.88 | | | | | | | |
| 1933 | 1.08 | 1.22 | 1.04 | 0.98 | 0.70 | 0.94 | 1.01 | | | | | | | |
| 1934 | 0.88 | 0.83 | 0.85 | 0.92 | 0.86 | 0.93 | 0.86 | | | | | | | |
| 1935 | 0.67 | 0.77 | 0.96 | 1.06 | 1.02 | 0.83 | 0.96 | | | | | | | |
| 1936 | 0.80 | 0.85 | 0.91 | 1.05 | 1.30 | 1.05 | 0.99 | | | | | | | |
| 1937 | 1.09 | 1.09 | 1.33 | 1.04 | 0.92 | 0.57 | 1.02 | | | | | | | |
| 1938 | 0.86 | 0.92 | 0.87 | 0.94 | 1.22 | 1.07 | 1.13 | | | | | | | |
| 1939 | 0.92 | 0.88 | 0.78 | 0.89 | 0.42 | 0.66 | 0.70 | | | | | | | |
| 1940 | 0.60 | 0.79 | 1.49 | 1.42 | 0.83 | 1.15 | 0.93 | | | | | | | |
| 1941 | 0.72 | 0.73 | 0.85 | 1.02 | 0.99 | 1.07 | 0.81 | | | | | | | |
| 1942 | 0.91 | 0.83 | 0.84 | 0.85 | 0.96 | 0.85 | 0.80 | | | | | | | |
| 1943 | 1.06 | 1.01 | 1.16 | 1.02 | 1.00 | 0.84 | 0.83 | | | | | | | |
| 1944 | 1.02 | 1.07 | 0.76 | 0.48 | 1.00 | 0.96 | 0.64 | | | | | | | |
| 1945 | 1.21 | 1.00 | 1.02 | 0.74 | 1.13 | 0.97 | 0.91 | | | | | | | |
| 1946 | 0.93 | 0.94 | 0.77 | 0.91 | 1.19 | 0.97 | 1.10 | | | | | | | |
| 1947 | 1.05 | 1.06 | 0.87 | 0.86 | 1.13 | 0.89 | 0.82 | | | | | | | |
| 1948 | 0.84 | 0.91 | 1.20 | 1.02 | 0.96 | 0.67 | 0.79 | | | | | | | |
| 1949 | 0.96 | 0.88 | 0.94 | 0.97 | 0.95 | 0.70 | 0.71 | | | | | | | |
| 1950 | 0.87 | 0.83 | 0.82 | 0.87 | 0.83 | 0.57 | 0.67 | 0.98 | 0.99 | 0.99 | 0.97 | 0.94 | 0.96 | 0.96 |
| 1951 | 1.11 | 1.02 | 1.34 | 1.43 | 1.33 | 1.28 | 1.41 | 1.01 | 0.98 | 1.03 | 1.03 | 1.05 | 1.06 | 1.05 |
| 1952 | 1.26 | 1.17 | 1.76 | 1.45 | 1.20 | 1.17 | 1.52 | 1.02 | 1.03 | 1.00 | 1.04 | 1.04 | 0.99 | 1.01 |
| 1953 | 1.18 | 1.09 | 0.80 | 0.87 | 0.29 | 0.43 | 0.41 | 0.97 | 1.01 | 0.96 | 0.98 | 0.94 | 0.96 | 0.93 |
| 1954 | 0.96 | 0.91 | 0.97 | 1.26 | 1.16 | 1.09 | 1.16 | 0.96 | 0.97 | 1.02 | 1.00 | 1.00 | 1.01 | 1.02 |
| 1955 | 1.35 | 1.38 | 1.41 | 1.27 | 1.08 | 0.91 | 0.69 | 1.03 | 1.03 | 1.02 | 1.03 | 1.02 | 1.04 | 0.96 |
| 1956 | 1.00 | 0.99 | 1.04 | 1.04 | 1.02 | 1.07 | 0.84 | 0.99 | 0.97 | 0.97 | 0.98 | 1.00 | 1.01 | 1.03 |
| 1957 | 0.71 | 0.79 | 1.02 | 0.85 | 0.85 | 0.92 | 0.95 | 0.99 | 0.97 | 1.01 | 0.98 | 0.99 | 1.00 | 0.95 |
| 1958 | 1.02 | 0.92 | 0.63 | 0.77 | 0.77 | 0.52 | 0.96 | 0.99 | 0.99 | 1.00 | 0.99 | 0.97 | 0.98 | 0.99 |
| 1959 | 1.01 | 1.02 | 1.52 | 1.52 | 1.76 | 1.44 | 1.52 | 1.01 | 1.02 | 1.04 | 1.04 | 1.04 | 1.07 | 1.08 |
| 1960 | 0.96 | 1.07 | 1.43 | 1.12 | 0.92 | 0.82 | 1.20 | 1.01 | 1.01 | 0.98 | 0.98 | 0.99 | 1.00 | 1.00 |
| 1961 | 0.97 | 1.00 | 0.77 | 0.82 | 0.85 | 0.79 | 0.61 | 0.97 | 0.98 | 0.99 | 0.98 | 1.00 | 0.97 | 0.94 |

| | | | | | | | | | | | | | | |
|---|---|---|---|---|---|---|---|---|---|---|---|---|---|---|
| 1962 | 1.00 | 0.86 | 1.16 | 1.22 | 1.45 | 1.27 | 1.21 | 0.99 | 1.00 | 1.01 | 1.03 | 1.03 | 1.06 | 1.08 |
| 1963 | 0.72 | 0.73 | 0.61 | 0.71 | 0.70 | 0.79 | 1.22 | 1.02 | 1.01 | 1.00 | 0.98 | 1.01 | 0.97 | 0.99 |
| 1964 | 1.13 | 1.09 | 1.11 | 0.97 | 1.26 | 1.13 | 1.16 | 0.98 | 0.99 | 0.96 | 0.96 | 0.98 | 0.99 | 1.01 |
| 1965 | 0.76 | 0.78 | 0.49 | 0.75 | 0.73 | 0.68 | 0.81 | 0.98 | 0.97 | 0.99 | 0.97 | 1.01 | 0.97 | 1.01 |
| 1966 | 0.91 | 0.99 | 1.00 | 1.09 | 1.15 | 1.12 | 1.40 | 1.01 | 1.01 | 1.03 | 1.02 | 0.97 | 1.03 | 1.03 |
| 1967 | 0.63 | 0.66 | 0.51 | 0.52 | 0.42 | 0.32 | 0.40 | 0.99 | 0.98 | 1.00 | 0.99 | 0.99 | 0.97 | 0.94 |
| 1968 | 1.13 | 1.06 | 1.10 | 1.18 | 1.15 | 1.23 | 0.88 | 1.01 | 1.02 | 1.00 | 1.00 | 1.03 | 1.01 | 1.04 |
| 1969 | 0.93 | 1.04 | 0.88 | 0.98 | 0.53 | 0.72 | 0.96 | 1.04 | 1.03 | 1.02 | 1.03 | 1.03 | 1.03 | 1.02 |
| 1970 | 0.99 | 0.95 | 0.86 | 0.91 | 0.61 | 0.59 | 0.96 | 0.98 | 1.01 | 0.99 | 1.00 | 1.03 | 0.96 | 0.98 |
| 1971 | 0.88 | 0.92 | 0.69 | 0.94 | 1.10 | 1.19 | 1.11 | 1.01 | 0.99 | 1.04 | 1.03 | 1.04 | 1.06 | 1.06 |
| 1972 | 1.04 | 1.08 | 1.03 | 1.04 | 1.26 | 1.30 | 1.38 | 1.04 | 1.05 | 1.04 | 1.05 | 1.03 | 1.04 | 1.04 |
| 1973 | 1.00 | 1.16 | 1.33 | 1.11 | 0.97 | 0.91 | 1.22 | 1.02 | 1.01 | 1.01 | 0.97 | 1.00 | 0.99 | 1.00 |
| 1974 | 0.96 | 1.00 | 0.56 | 0.77 | 0.89 | 0.86 | 0.81 | 1.03 | 1.03 | 1.00 | 1.03 | 1.00 | 1.01 | 1.02 |
| 1975 | 0.94 | 0.89 | 0.87 | 1.01 | 1.02 | 0.93 | 1.06 | 1.01 | 1.00 | 1.04 | 1.02 | 1.00 | 1.01 | 0.98 |
| 1976 | 1.38 | 1.44 | 1.36 | 1.44 | 1.78 | 1.62 | 1.16 | 1.04 | 1.04 | 0.99 | 1.04 | 1.02 | 1.03 | 1.06 |
| 1977 | 0.85 | 1.09 | 1.66 | 1.42 | 1.25 | 1.25 | 1.55 | 1.04 | 1.03 | 1.05 | 1.01 | 0.99 | 0.99 | 1.04 |
| 1978 | 0.85 | 0.83 | 1.08 | 0.82 | 0.82 | 0.92 | 0.90 | 0.97 | 0.97 | 0.98 | 1.03 | 1.00 | 0.99 | 0.98 |
| 1979 | 1.03 | 1.06 | 0.88 | 0.94 | 0.65 | 0.90 | 0.61 | 1.02 | 1.01 | 0.98 | 0.96 | 1.00 | 0.97 | 0.99 |
| 1980 | 1.11 | 1.07 | 1.16 | 1.24 | 1.41 | 1.31 | 1.38 | 0.99 | 0.98 | 1.00 | 1.02 | 1.01 | 0.96 | 1.02 |
| 1981 | 1.11 | 1.15 | 0.74 | 0.67 | 0.64 | 0.61 | 0.52 | 1.01 | 0.98 | 0.97 | 0.96 | 0.97 | 0.98 | 0.93 |
| 1982 | 1.00 | 1.09 | 0.96 | 1.01 | 0.94 | 0.98 | 0.86 | 0.99 | 0.99 | 0.97 | 0.94 | 0.96 | 0.94 | 0.95 |
| 1983 | 1.08 | 1.03 | 0.59 | 0.69 | 0.70 | 0.86 | 1.07 | 1.00 | 0.98 | 0.96 | 0.99 | 0.94 | 0.93 | 0.97 |
| 1984 | 0.82 | 0.69 | 0.73 | 0.96 | 1.02 | 0.97 | 0.75 | 0.97 | 0.99 | 0.99 | 0.91 | 1.01 | 1.01 | 0.99 |
| 1985 | 1.14 | 1.12 | 1.00 | 1.04 | 1.04 | 0.95 | 0.81 | 1.02 | 1.00 | 0.99 | 1.00 | 1.00 | 0.98 | 0.98 |
| 1986 | 0.96 | 0.87 | 1.12 | 0.98 | 0.47 | 0.54 | 0.37 | 1.00 | 0.99 | 0.98 | 0.98 | 0.97 | 0.98 | 0.93 |
| 1987 | 0.82 | 0.86 | 0.56 | 0.64 | 1.11 | 0.75 | 1.01 | 1.01 | 1.00 | 0.97 | 0.97 | 0.97 | 1.00 | 0.99 |
| 1988 | 0.81 | 0.83 | 1.01 | 1.02 | 1.43 | 1.52 | 1.51 | 1.02 | 1.03 | 1.01 | 1.05 | 1.01 | 1.06 | 1.07 |
| 1989 | 1.11 | 1.03 | 1.39 | 1.27 | 1.19 | 1.32 | 1.53 | 1.04 | 1.02 | 1.02 | 0.99 | 1.02 | 1.01 | 1.07 |
| 1990 | 1.00 | 0.85 | 1.08 | 0.92 | 1.10 | 1.20 | 0.93 | 1.00 | 1.01 | 0.97 | 1.01 | 0.99 | 0.99 | 0.99 |
| 1991 | 0.82 | 0.75 | 0.80 | 0.99 | 0.88 | 1.18 | 0.54 | 1.00 | 0.99 | 1.02 | 1.02 | 1.01 | 1.02 | 0.98 |
| 1992 | 1.17 | 1.27 | 0.75 | 1.34 | 0.67 | 0.88 | 0.85 | 1.01 | 1.02 | 1.03 | 0.99 | 0.99 | 0.97 | 0.96 |
| 1993 | 0.97 | 0.89 | 0.82 | 0.99 | 0.98 | 0.88 | 0.71 | 1.00 | 0.98 | 1.01 | 0.98 | 0.99 | 0.99 | 0.97 |
| 1994 | 0.79 | 0.83 | 0.58 | 0.48 | 0.27 | 0.13 | 0.40 | 0.99 | 0.99 | 1.00 | 1.01 | 0.99 | 0.95 | 0.93 |
| 1995 | 1.03 | 1.09 | 0.99 | 0.81 | 1.04 | 0.87 | 1.48 | 1.02 | 1.01 | 0.98 | 0.98 | 0.97 | 0.96 | 0.99 |
| 1996 | 0.94 | 0.88 | 1.03 | 0.88 | 1.16 | 1.24 | 1.07 | 1.00 | 1.02 | 1.02 | 1.03 | 1.03 | 1.02 | 1.00 |
| 1997 | 1.12 | 1.09 | 1.36 | 1.01 | 1.13 | 1.71 | 1.68 | 1.03 | 1.03 | 0.98 | 1.01 | 1.00 | 1.02 | 1.05 |
| 1998 | 0.94 | 0.95 | 0.83 | 0.83 | 0.81 | 0.93 | 0.91 | 0.97 | 0.98 | 1.00 | 1.02 | 1.01 | 1.00 | 0.98 |
| 1999 | 1.06 | 1.10 | 0.88 | 0.96 | 1.11 | 1.15 | 1.10 | 1.00 | 0.99 | 1.01 | 1.00 | 0.99 | 1.00 | 0.99 |
| 2000 | 1.32 | 1.26 | 1.40 | 1.21 | 1.18 | 1.30 | 0.85 | 0.98 | 0.99 | 1.00 | 1.00 | 1.03 | 1.03 | 0.98 |
| 2001 | 0.80 | 0.73 | 1.08 | 0.87 | 0.60 | 0.61 | 1.29 | 0.98 | 0.98 | 0.99 | 0.98 | 0.99 | 0.98 | 1.02 |
| 2002 | 1.10 | 1.18 | 1.04 | 1.02 | 1.17 | 1.49 | 1.13 | 1.02 | 1.00 | 1.02 | 1.00 | 1.03 | 1.01 | 1.00 |
| 2003 | 0.90 | 0.90 | 0.98 | 1.11 | 1.31 | 1.57 | 1.48 | 0.99 | 1.01 | 1.03 | 1.04 | 1.04 | 1.04 | 1.03 |
| 2004 | 0.99 | 0.88 | 1.09 | 1.26 | 1.48 | 1.42 | 1.13 | 0.97 | 0.98 | 1.01 | 1.01 | 0.99 | 1.02 | 0.97 |
| 2005 | 1.31 | 1.23 | 0.81 | 0.54 | 0.13 | 0.35 | 0.10 | 0.97 | 0.97 | 0.96 | 0.92 | 0.97 | 0.95 | 0.98 |
| 2006 | 1.40 | 1.36 | 0.92 | 1.14 | 1.37 | 0.97 | 1.14 | 1.00 | 1.01 | 0.98 | 1.00 | 0.94 | 0.99 | 1.00 |
| 2007 | 0.73 | 0.83 | 1.07 | 1.34 | 1.53 | 1.47 | 1.52 | 1.01 | 1.00 | 1.04 | 1.04 | 1.04 | 1.04 | 1.03 |
| 2008 | 1.15 | 1.04 | 1.77 | 1.57 | 1.34 | 1.56 | 1.19 | 1.00 | 0.99 | 1.00 | 1.02 | 1.00 | 1.01 | 1.02 |
| 2009 | 0.98 | 0.87 | 0.66 | 0.67 | 0.80 | 0.93 | 0.82 | 0.96 | 0.97 | 0.99 | 0.99 | 1.01 | 1.02 | 1.01 |
| 2010 | 1.58 | 1.52 | 1.36 | 1.51 | 1.47 | 1.85 | 1.14 | 1.00 | 1.03 | 1.02 | 1.02 | 1.03 | 1.03 | 1.04 |
| 2011 | 1.41 | 1.26 | 1.56 | 1.44 | 1.21 | 1.09 | 0.79 | 0.99 | 1.01 | 1.02 | 1.00 | 1.00 | 1.01 | 1.01 |

**Supplementary Figures**

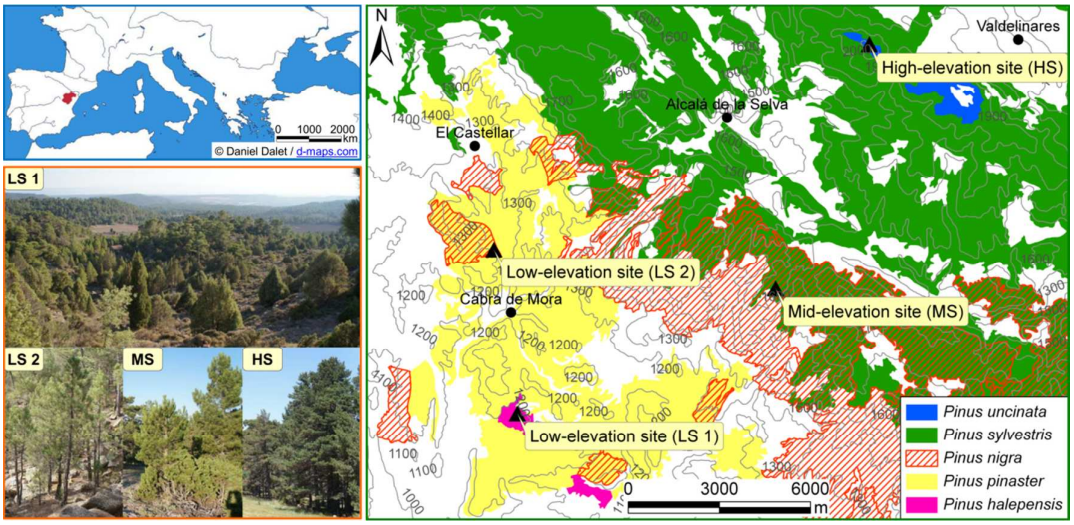


**Figure S1**. Location of the study area (top left) and topography and distribution of pine stands in the Gúdar mountain range (right). Photographs (centre left, down left) show the stand conditions at each sampling site.

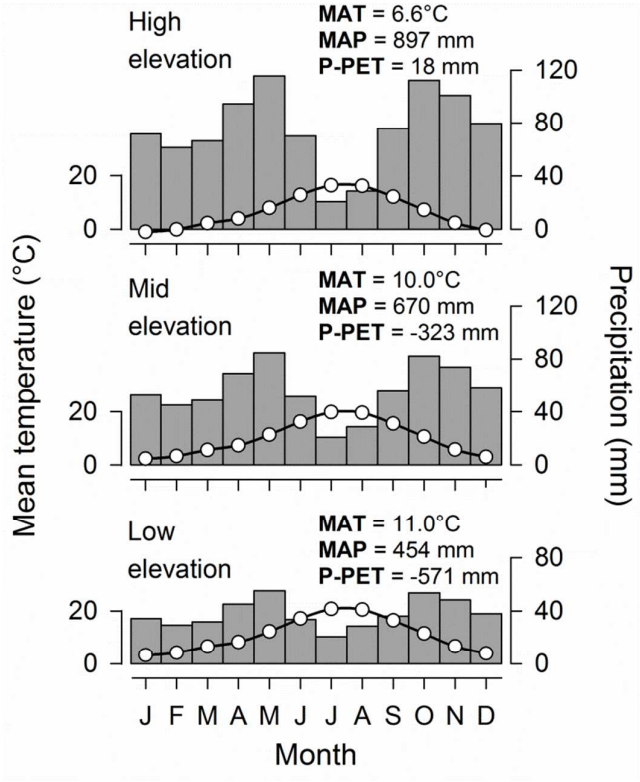


**Figure S2**. Climate diagrams corresponding to low- (LS), mid- (MS) and high-elevation (HS) sites. The primary *y*-axis indicates monthly mean temperature (lines) and the secondary *y*-axis monthly precipitation (bars). Average monthly values of climate factors were estimated based on the European high-resolution climate dataset (E-OBS) for the period 1980–2011. The mean annual temperature (MAT), mean annual precipitation (MAP) and annual water availability (the difference between precipitation and potential evapotranspiration; P-PET) are given for each elevation belt.

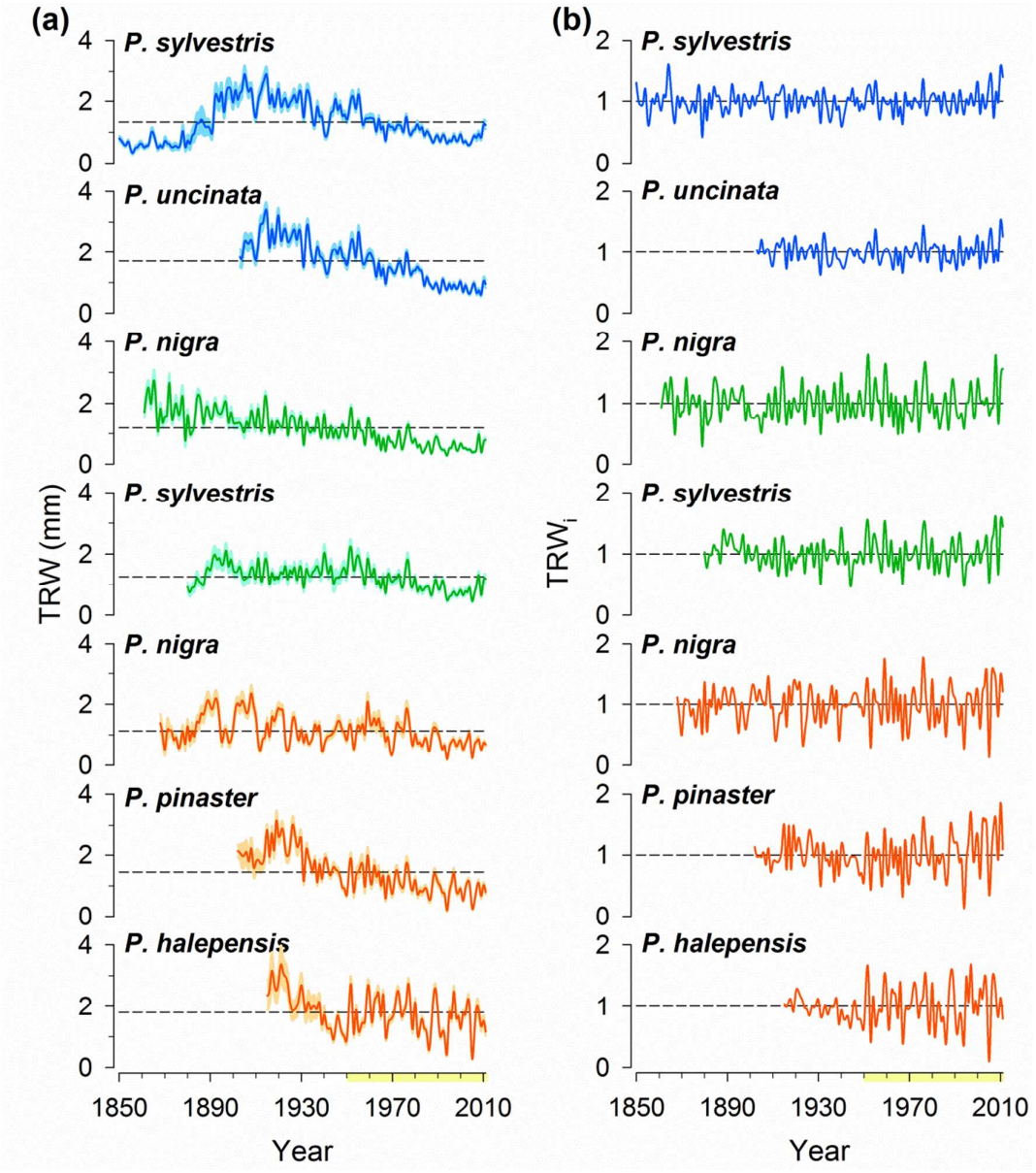


**Figure S3**. Raw (non-standardised) (a) and indexed (spline of 100 year length) (b) tree-ring width (TRW) chronologies for every site-species combination. Blue lines refer to the high-elevation site (HS), green lines to the mid-elevation site (MS) and red lines to the low-elevation sites (LS). Shaded areas denote standard errors. All individual chronologies were truncated for intervals for which the Expressed Population Signal (EPS) was lower than 0.85 (values of *EPS* higher than 0.85 are usually regarded as representing well-replicated chronologies). The dashed lines indicate mean values of each chronology (absolute TRW, left panels; indexed $TRW_i$, right panels). The yellow area in the *x*-axis corresponds to years with available $\Delta^{13}$C records.

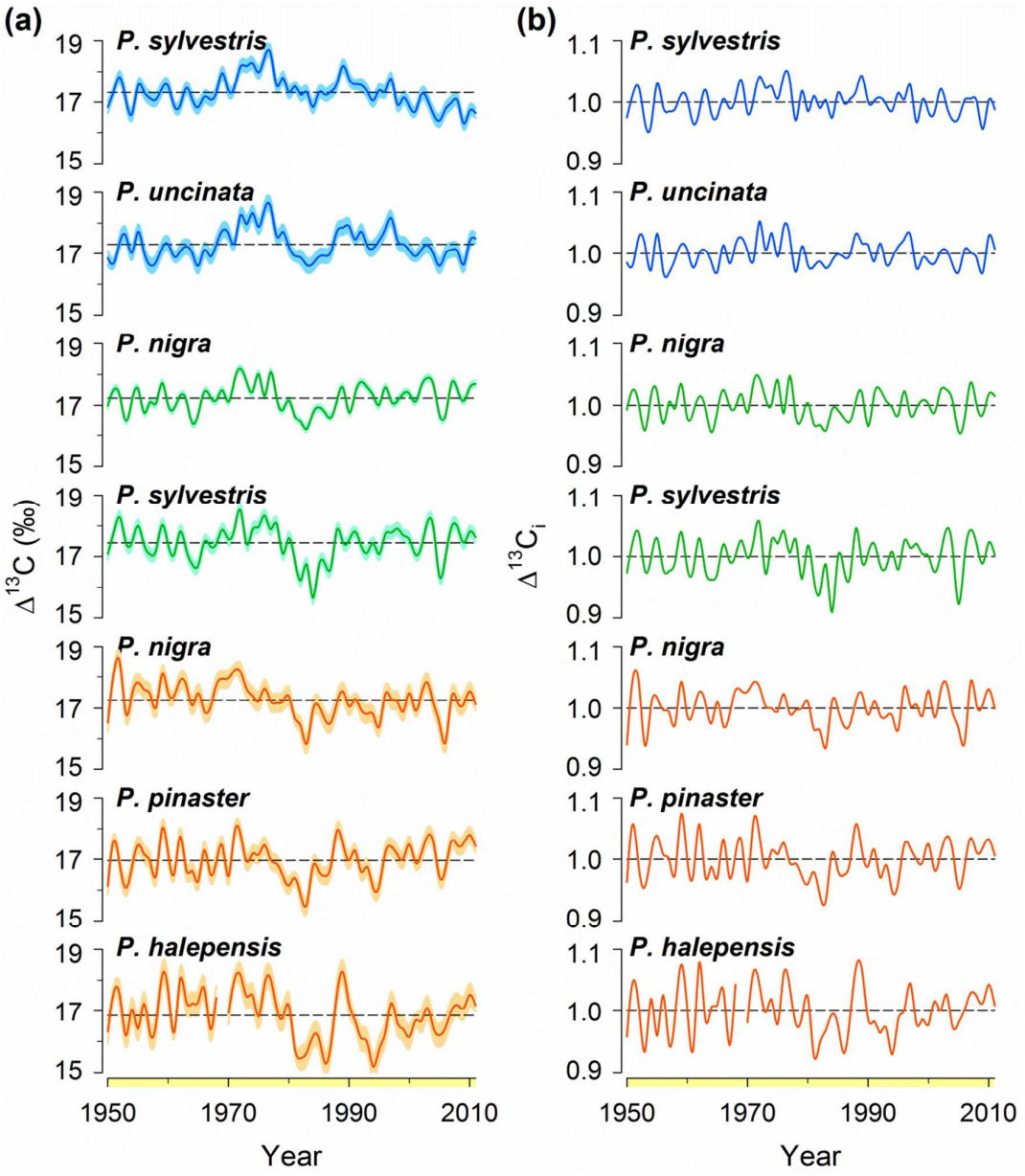


**Figure S4**. Raw (non-standardised) (a) and indexed (b) carbon isotope discrimination ($\Delta^{13}$C) chronologies for every site-species combination for the period 1950–2011. Blue lines refer to the high-elevation site (HS), green lines to the mid-elevation site (MS) and red lines to the low-elevation sites (LS). Shaded areas denote standard errors. The dashed lines indicate mean values of each chronology (original $\Delta^{13}$C, left panels; indexed $\Delta^{13}C_i$, right panels).

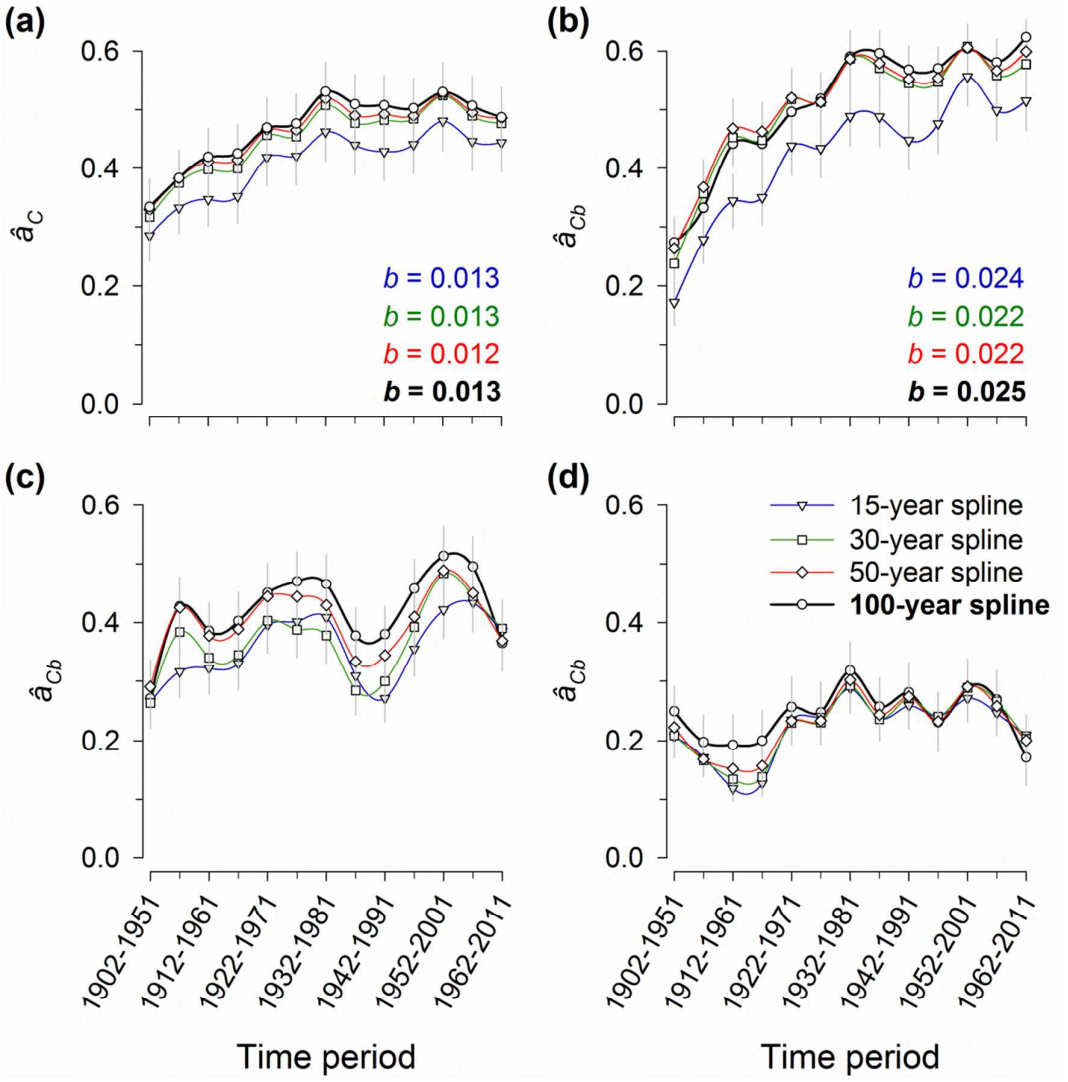


**Figure S5.** Temporal trends in spatial synchrony along the altitudinal gradient estimated for 50-year periods lagged by five years (period 1902–2011). Trends are shown for all chronologies together ($\hat{a}_C$) (eqn 6, Supplementary details on statistical analysis of this Appendix) (a), and also for pairs of chronologies belonging to different altitudinal belts ($\hat{a}_{Cb}$) (eqn 7, idem) as follows: low-elevation *vs*. mid-elevation chronologies (b), mid-elevation *vs*. high-elevation (c), and low-elevation *vs*. high-elevation (d). Thick black lines depict trends obtained after spline detrending with length = 100 years, red lines with length = 50 years, green lines with length = 30 years and blue lines with length = 15 years. Significant linear trends of $\hat{a}_C$ and $\hat{a}_{Cb}$ values over time are identified with their corresponding slope estimate ($P < 0.05$).

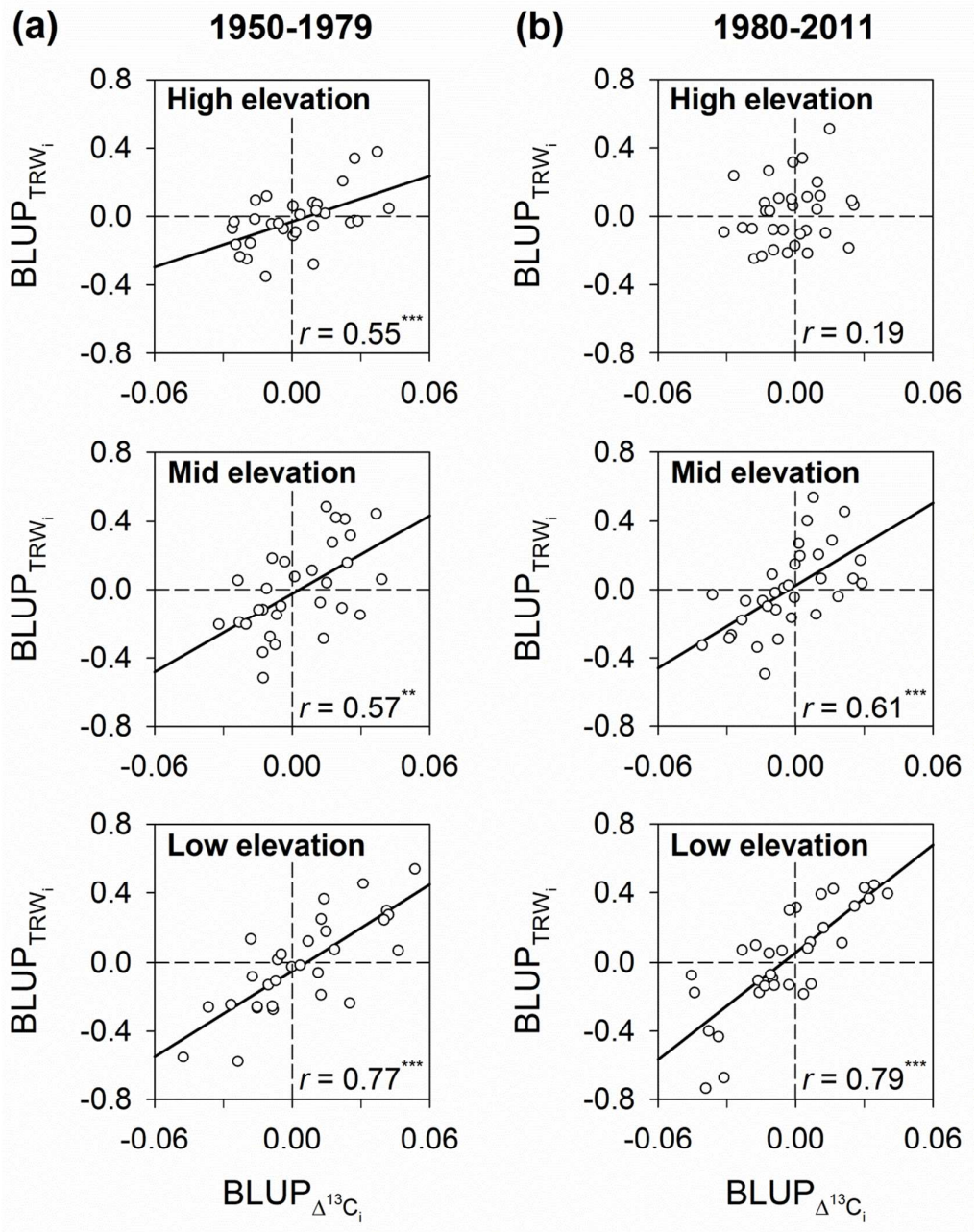


**Figure S6.** Relationships between indexed tree-ring width ($TRW_i$) and carbon isotope discrimination ($\Delta^{13}C_i$) records along the altitudinal gradient. The correlations are estimated using best linear unbiased predictors (BLUPs) of year effects ($\Delta^{13}C_i$, *x*-axis; $TRW_i$, *y*-axis) for two consecutive periods: (a) 1950–1979 and (b) 1980–2011. Significant linear associations are depicted as black lines ($^{**}$ $P < 0.01$; $^{***}$ $P < 0.001$).

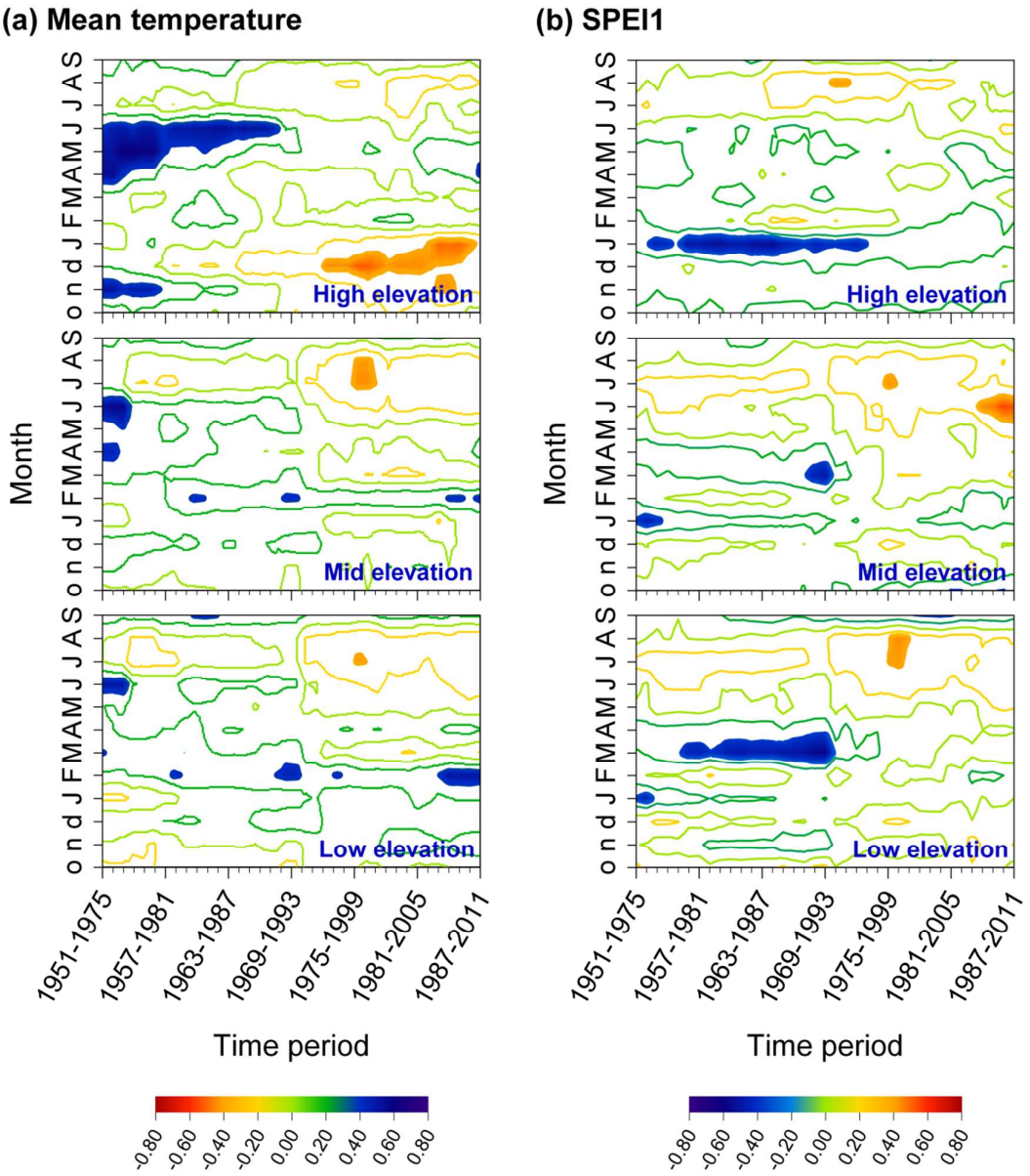


**Figure S7.** Moving correlations (after controlling for the effect of indexed carbon isotope discrimination [$\Delta^{13}C_i$] through partial correlation analysis) between indexed ring-width chronologies ($TRW_i$) and monthly mean temperature (a) and precipitation (b) for each altitudinal belt (period 1950–2011). The threshold for significance is $r$ = ±0.41 ($n$ = 25; $d.f.$ = 22; $P < 0.05$). Non-filled areas denote non-significant correlations. Lowercase and uppercase letters in the $y$-axes correspond to months of the years before and during tree-ring formation, respectively.

**References**

Cook, E.R. & Krusic, P.J. (2005) *Program ARSTAN: A treering standardization program based on detrending and autoregressive time series modeling, with interactive graphics*. Columbia University, Palisades, New York.

Farquhar, G.D., Ehleringer, J. & Hubick, K. (1989) Carbon isotope discrimination and photosynthesis. *Annual Review of Plant Physiology and Plant Molecular Biology*, **40**, 503–537.

Gandullo, J.M. (1994) *Climatología y ciencia del suelo*. Fundación Conde del Valle de Salazar, Madrid.

Gilmour, A.R., Gogel, B.J., Gullis, B.R., Welham, S.J. & Thompson, R. (2002) *ASReml user guide release 1.0*. VSN International Ltd, Hemel Hempstead.

Haylock, M.R., Hofstra, N., Klein Tank, A.M.G., Klok, E.J., Jones, P.D. & New, M. (2008) A European daily high-resolution gridded dataset of surface temperature and precipitation. *Journal of Geophysical Research*, **113**, D20119.

Herrera, S., Fita, L., Fernández, J. & Gutiérrez, J. (2010) Evaluation of the mean and extreme precipitation regimes from the ENSEMBLES regional climate multimodel simulations over Spain. *Journal of Geophysical Research*, **115**, D21117.

Saurer, M., Siegwolf, R., Schweingruber, F. (2004) Carbon isotope discrimination indicates improving water-use efficiency of trees in northern Eurasia over the last 100 years. *Global Change Biology*, **10**, 2109–2120.

Shestakova, T.A., Aguilera, M., Ferrio, J.P., Gutiérrez, E. & Voltas, J. (2014) Unravelling spatiotemporal tree-ring signals in Mediterranean oaks: a variance-covariance modelling approach of carbon and oxygen isotope ratios. *Tree Physiology*, **34**, 819–838.

White, T.L. & Hodge, G.R. (1989) *Predicting breeding values with applications in forest tree improvement*. Kluwer Academic Publisher, Dordrecht.

Wigley, T.M.L., Briffa, K.R. & Jones, P.D. (1984) On the average of correlated time series, with applications in dendroclimatology and hydrometeorology. *Journal of Climate and Applied Meteorology*, **23**, 201–213.